medRxiv preprint doi: https://doi.org/10.1101/2022.03.08.22272025; this version posted March 10, 2022. The copyright holder for this preprint (which was not certified by peer review) is the author/funder, who has granted medRxiv a license to display the preprint in perpetuity.
It is made available under a CC-BY-NC-ND 4.0 International license .

# Integrated single-cell RNA sequencing analysis reveals alterations of ageing human lung endothelium heterogeneity in idiopathic pulmonary fibrosis

Eamon C. Faulkner[1], Adam A. Moverley[2], Simon P. Hart[3,4*] and Leonid L. Nikitenko[1*#]

[1]Department of Biomedical Sciences and [3]Respiratory Research Group, Hull York Medical School, University of Hull; [2]Department of Cell and Developmental Biology, University College London, [4]Hull University Teaching Hospitals NHS Trust. [*]Authors share senior authorship. [#]Corresponding author: l.nikitenko@hull.ac.uk

**Running title:** Heterogeneity of ageing human lung endothelium and its alterations in idiopathic pulmonary fibrosis

**Keywords:** ageing lung, endothelial cell, lymphatic, idiopathic pulmonary fibrosis, single cell RNA sequencing.

## ABSTRACT

Increasing age is the main risk factor for chronic lung diseases (CLD) including idiopathic pulmonary fibrosis (IPF). Halting or reversing progression of IPF remains an unmet clinical need due to limited knowledge of underlying mechanisms. In particular, the contribution of the endothelium to ageing in human lung under physiological conditions and in IPF remains insufficiently understood. In this study, we analysed heterogeneity of endothelium in physiologically ageing human lung and its alterations in IPF. We conducted a comprehensive *in silico* analysis of scRNAseq profiles of human lung tissues from older healthy donors and age-matched IPF patients (n=9 for each group) by integrating datasets from two independent cohorts. We generated a single-cell map of the ageing human lung and identified 17 subpopulations of ageing endothelium (12 for blood and 5 for lymphatic vessels, including 4 "de-differentiated"), with distinct transcriptional profiles, specific gene expression signatures and percentage contributions, revealing previously underappreciated extent of heterogeneity. In IPF lung, the balance of different endothelial sub-types was significantly altered both in terms of cell numbers and gene expression patterns, identifying disease-relevant subpopulations and transcriptional changes associated with specific signalling pathways and cellular processes. These findings reveal a previously unrecognised phenomenon of ageing human lung endothelium re-programming towards an "IPF endothelium" state, suggesting potential avenues for therapeutic management or biomarker discovery for diagnostics or prognostics of IPF. Our study creates a conceptual framework for appreciating the heterogeneity of ageing endothelium and its alterations in CLDs and diseases associated with fibrosis in other organs, including lymphoedema and cancer.

**NOTE: This preprint reports new research that has not been certified by peer review and should not be used to guide clinical practice.**

medRxiv preprint doi: https://doi.org/10.1101/2022.03.08.22272025; this version posted March 10, 2022. The copyright holder for this preprint (which was not certified by peer review) is the author/funder, who has granted medRxiv a license to display the preprint in perpetuity.
It is made available under a CC-BY-NC-ND 4.0 International license .

## INTRODUCTION

Increasing age is the main risk factor for diagnosis and prognosis of major non-communicable diseases, including chronic lung diseases (CLDs), such as most forms of lung cancer, chronic obstructive pulmonary disease (COPD) and idiopathic pulmonary fibrosis (IPF) (1). IPF is the most common, progressive and lethal interstitial lung disease with a prevalence rate of 33 to 450 per million people globally (2). IPF progression leads to declining quality of life, respiratory failure and eventually lung transplantation or death. IPF is characterised by a histopathological pattern of usual interstitial pneumonia (UIP), comprising spatially and temporally heterogeneous deposition of collagens and other extracellular matrix (ECM) proteins within the alveolar walls, fibroblastic foci, and architectural distortion of the lung with cystic honeycomb change and fibrosis (3). While the number of older people suffering from IPF is steadily increasing, and hallmarks of ageing, particularly cellular senescence and ECM dysregulation, are prominent in the IPF lung, the aetiology of this disease remains unclear (4-6). Detailed understanding of cellular and molecular mechanisms underlying IPF-associated changes in ageing human lung will be essential for developing effective therapies to halt or reverse disease progression in elderly patients.

Several lines of evidence implicate a role for the circulatory system, composed of blood vascular and lymphatic vessel networks, in IPF (7-17). Some of these studies highlight structural and functional features of blood and lymphatic vessels, which are lined with a monolayer of endothelial cells (EC, or endothelium), in IPF lung, although often without a reference to or comparison between patients and age-matched controls/healthy donors (9, 14, 16). Furthermore, the lung has two distinct blood vascular circulatory networks – (bronchial and pulmonary; (18)) and three main networks of lymphatic vessels - in pulmonary tissue (peribronchial and perivascular - running parallel to the major airways and respiratory bronchioles, and existing in close proximity to the intralobular arterioles and small veins, or associated with alveoli) and in subpleural space (draining lymph from the surface of the organ) (19). The precise contribution of these specialised networks and the vessel subtypes and EC subpopulations that comprise them, to the pathophysiology and progression of IPF, or other CLDs, remain insufficiently characterised, except few individual studies (20, 21).

Recent advances in single-cell RNA sequencing (scRNAseq) and big data analysis (22) have allowed characterisation of cellular heterogeneity in healthy and diseased lung, resulting in the generation of a human lung cell atlas (HLCA; (21)) and the IPF cell atlas (23). Several studies have also focused on dissecting phenotypic heterogeneity of human lung endothelium, using single cell transcriptional profiling, identifying six or nine subpopulations of EC in healthy and/or diseased lung (21, 24, 25). These reports utilised data from either a diverse population of subjects (patients with IPF, COPD or other interstitial lung diseases, commonly placed together for comparison) with a range of ages (varying from 21 to 80 years in some cases), ethnicities and tobacco smoker statuses, or used samples from different areas of the lung, e.g. distal lung parenchyma (26), longitudinal sections (24) or multiple lobes (27). The most recent study generated cell atlases of the COPD lung for both human and murine tissues, comparative to physiologically ageing controls, identifying 6 subpopulations of EC (20). However, to date no comparison of lung endothelium has been performed between elderly IPF patients and age-matched healthy individuals. As a result, currently there is a major gap in knowledge about the sub-types, properties and roles of ageing human lung endothelium in physiological conditions, IPF and other CLD including lung cancer.

In this study, we have conducted the first comprehensive comparative *in silico* analysis of scRNAseq profiles of human lung tissues obtained from IPF patients and age-matched donors (49-72 years old for both groups) by integrating datasets from two independent cohorts, each composed of healthy and IPF lung datasets (24, 26). We generated a single-cell map of ageing human lung, identified 17 subpopulations of ageing lung endothelium (12 and 5 for blood and

medRxiv preprint doi: https://doi.org/10.1101/2022.03.08.22272025; this version posted March 10, 2022. The copyright holder for this preprint (which was not certified by peer review) is the author/funder, who has granted medRxiv a license to display the preprint in perpetuity.
It is made available under a CC-BY-NC-ND 4.0 International license .

lymphatic vessel EC respectively) and characterised their transcriptional profiles, differences in percentage contribution and gene expression signatures. These findings reveal previously under-appreciated extent of heterogeneity of human ageing lung endothelium and its alterations (both in terms of gene expression profiles and percentage contributions of individual subpopulations of EC) in IPF patients, resulting in re-modelling towards an "IPF endothelium" state.

## RESULTS

### *Integrated single-cell RNA sequencing analysis reveals endothelial cell contribution to ageing human lung tissue microenvironment in IPF.*

To enable comprehensive scRNAseq data analysis of ageing human lung endothelium in IPF and to account for intra- and inter-lung heterogeneity (within and between individuals; (28)), we selected data from only those studies that contained lung tissues from both IPF patients and age-matched (49-72 years old) healthy donors. From all publicly available scRNAseq datasets of human IPF lungs (4 in total), only two, representing independent cohorts of subjects/individuals of different ethnic backgrounds, fulfilled these selection criteria and were used for generating a single dataset for integrative analysis (24, 26). Four age-matched pairs (scRNAseq data from lung tissue samples from transplantation stage IPF patients and healthy donors) from the first database (26) matched our selection criteria and formed cohort 1 (Table 1, Figure 1A). Five age-matched pairs from the second database (32 IPF and 28 donor samples ranging from 21 to 80 years old, (24)), matching our selection criteria and forming cohort 2, were randomly selected for the integrated analysis in order to correspond to the number of cells analysed from cohort 1 (Table 1, Figure 1A). In these two cohorts, the overall protocol for cell extraction and processing for scRNAseq was similar, but tissue samples were collected from different regions of the lung. Peripheral distal lung tissue (parenchyma; 1-2cm) was used in cohort 1 and longitudinal sections in cohort 2 samples. The summary of the information on cohort-specific patient characteristics and lung tissue collection sites is outlined in Table 1, with more detailed information on sample preparation in the two datasets available in Materials and Methods. The collection from different regions across the lung presented the ideal platform to account for heterogeneity of tissue composition within and between the individual lungs included in our integrated analysis.

Clustering analysis of ageing human lung tissue in each cohort identified two closely related clusters of ageing blood and lymphatic vessel EC (BEC and LEC respectively) in both (Supplementary Figure 1 A), with their cluster identity confirmed by expression of EC-specific markers, including *VWF* (for BEC), prospero homeobox 1 (*PROX1*; for LEC) and calcitonin-receptor-like receptor (*CALCRL*; pan-EC) (Supplementary Figure 1 B; (29-32)) and others (see Materials and Methods). Unsupervised sub-clustering analysis of the total ageing human lung endothelium (BEC and LEC pooled together) revealed 5 sub-populations of EC in cohort 2, closely matching COPD cell atlas data that compared ageing-matched datasets of human lung and identified 6 sub-populations of EC (20) Supplementary Figure 1 C). In contrast, unexpectedly 12 sub-populations of ageing human lung EC were identified in cohort 1, potentially reflecting the differences in sample collection sites (Table 1). All EC sub-populations had distinct gene expression profiles in both cohorts (Supplementary Figure 1 D, E).

Next, the integration of two datasets into one, accounting for intra- and inter-lung heterogeneity of EC in the ageing human lung and IPF-associated alterations, resulted in generation of a novel single cell map and revealing the presence of 25 distinct cell clusters (Figures 1 A and B), based on specific gene expression patterns (Figure 1 C and Supplementary Figure 2 A, Supplementary Table 1) that express cell type-specific markers proposed in

medRxiv preprint doi: https://doi.org/10.1101/2022.03.08.22272025; this version posted March 10, 2022. The copyright holder for this preprint (which was not certified by peer review) is the author/funder, who has granted medRxiv a license to display the preprint in perpetuity.
It is made available under a CC-BY-NC-ND 4.0 International license .

previous studies (21, 24-26). Distinct identities of two closely related BEC and LEC clusters (11 and 20; Figure 1 B) were confirmed by focused in-depth analysis of expression of a panel of EC markers *VWF*, platelet endothelial cell adhesion molecule-1 (*PECAM1*), vascular endothelial cadherin (*CDH5* or VE-cadherin) and *CALCRL*, and lymphatic vessel EC-specific genes (*PROX1*, *PDPN*, lymphatic vessel endothelial hyaluronan receptor 1, *LYVE-1*, and fms-related receptor tyrosine kinase 4, *FLT4*; Figure 1 D) (29-32).

Quantitative analysis of the cell numbers for each of 25 clusters in age-matched groups revealed IPF-associated changes in ageing human lungs in both cohorts (Figure 1 E). This reflects differences in location of tissue samples collected for scRNAseq analysis (Table 1) and matches reported in non-age matching studies contribution of different cell types to the total human lung cell population and alterations in IPF lung (20, 21, 24-26, 33, 34) Supplementary Table 2). Our data also uncovered changes in proportions of ageing human lung BEC and LEC populations between cohorts and conditions (Figure 1 E, Supplementary Table 3). Data integration revealed the comparable spatial profiles and contribution of ageing human lung EC populations in donor and fibrosis, and in individual cohorts (Figure 1F). Quantitative analysis demonstrated the similarity in contribution of ageing human lung EC populations in integrated dataset to two conditions (donor and IPF; Figure 1 G).

In summary, the comprehensive analysis of scRNAseq profiles of human lung tissues from elderly healthy donors and age-matched IPF patients by integrating datasets from two independent cohorts enabled the generation of a novel map of individual cell populations in ageing human lung and identification of ageing human lung endothelium from blood and lymphatic vessels. This data provides a foundation for studying changes in transcriptional profiles and contribution of these cell populations, especially endothelium, within ageing human lung in IPF and other age-associated lung diseases.

***Integrated single-cell RNA sequencing analysis reveals heterogeneity of blood vessel endothelial cell population in ageing human lung tissue microenvironment and IPF-associated alterations in cell numbers within individual sub-populations.***

Next, to comprehensively decipher transcriptional signatures of ageing human lung blood vessel endothelium in IPF, we subtracted scRNAseq data for ageing human lung BEC (n=3192) from the total lung cell populations from integrated dataset (two cohorts and both conditions), and sub-clustered them (Figure 1A; Figure 2 A). Unsupervised clustering identified 12 distinct sub-clusters of ageing human lung BEC (0-11; Figure 2 A), based on their differential gene expression (DEG) patterns (top 10 DEG for each, 120 in total; Figure 2 B and Supplementary Figure 3). This finding revealed previously under-appreciated extent of diversity of ageing human lung BEC sub-types (and hence heterogeneity of BEC population) in ageing human lung. Expression analysis of pan-EC markers and LEC-specific genes (Figure 2 C) confirmed the identities of these subpopulations as BEC.

The analysis of the top 10 DEG for each sub-cluster (120 in total; Figure 2 B; Supplementary Figures 3 and 4; Supplementary Table 4), when performed alongside tests for expression of pan-EC and LEC markers (Figure 2 C) and using violin plots to test their sub-clusters-specific expression (Supplementary Figure 3), determined their selection for inclusion (or not) in 10 signatures of ageing lung endothelium sub-populations (Figure 2 D). 50 selected sub-cluster-specific genes contribute to distinct transcriptional profiles for sub-clusters 1-4 and 6-11 (Figure 2 D) and represent candidate genes for further investigation of their roles in individual BEC subpopulations in ageing human lung. Sub-clusters 0 and 5 lack obvious markers or signatures (Figure 2 D; Supplementary Figure 5).

Three-dimensional pseudo-time lineage analysis of scRNAseq/transcriptional profiles of all 12 identified ageing human lung BEC sub-clusters revealed close relationships between them (Figure 2 E; Supplementary Video 1). This included a direct link between sub-cluster 5 and

medRxiv preprint doi: https://doi.org/10.1101/2022.03.08.22272025; this version posted March 10, 2022. The copyright holder for this preprint (which was not certified by peer review) is the author/funder, who has granted medRxiv a license to display the preprint in perpetuity.
It is made available under a CC-BY-NC-ND 4.0 International license .

sub-cluster 3, and manifestation of sub-cluster 0 as a "convergence point" for 7 other sub-clusters (1, 2, 4, 6, 9, 10 and 11). When applied to 12 ageing human lung BEC subpopulations, the dot plot expression analysis of markers of lung EC sub-types proposed in other transcriptional studies in human and murine tissues (35-40) identified few distinct matches (Supplementary Figure 7). Further exploration of identities of 12 sub-populations by using these markers alongside those proposed for specific EC sub-clusters in HLCA and IPF cell atlas studies (20, 21, 23-25), when coupled with module scoring (Figure 2 F) and cell cycle (Supplementary Figure 8) analyses, confirmed these matches, whilst 4 sub-clusters remained unannotated (Figure 2 F; Supplementary Figure 7). Altogether, these findings (Figure 2; Supplementary Figure 7) suggest that our study de-convoluted ageing human lung BEC population, providing advanced resolution of its heterogeneity at a transcriptional level, increasing the number of EC sub-clusters (20, 21) and revealing previously underappreciated extend of diversity of ageing blood endothelium in human lung.

Quantitative analysis of percentage contribution of cells from each sub-cluster to total BEC population in ageing human lung from healthy donors and IPF patients revealed a significant increase in representation of two sub-clusters (1 and 2) and decrease in sub-cluster 7 in IPF (Figure 3 A-C; Supplementary Table 5), and their specificity by the cohort (Figure 3 D). These findings therefore also reveal substantial alterations in cell numbers within individual sub-clusters of ageing human lung BEC in IPF.

In summary, our study is the first to create a novel single-cell map of the ageing human lung blood vessel endothelium and identify 12 sub-clusters of BEC with distinct transcriptional profiles, individual gene and expression signatures and percentage contribution in donors and IPF patients. This knowledge provides a foundation for studying specific roles of these sub-populations of BEC within ageing human lung in IPF and could be critical to understanding pathophysiology of this and other age-associated lung diseases.

***Annotation of blood vessel endothelial cell subpopulations in ageing human lung reveals their differentiation status, associations with bronchial or pulmonary capillary networks and IPF-associated alterations.***

The profiling of markers of EC sub-types (Figure 2 F; Supplementary Figure 6 and 7), when combined with the expression of pan-EC and LEC markers (Figure 2 C, D) and sub-cluster-specific signatures identified in this study (based on expression pattern of 50 DEG; Figure 2 D; Supplementary Figure 3), cell cycle analysis data (Supplementary Figure 8), findings from three-dimensional pseudo-time lineage analysis (Figure 2E, Supplementary Video 1), quantification of percentage contribution (Figure 3) and lung tissue sample collection locations (Table 1), formed the foundation for the annotation of 12 identified ageing human lung BEC sub-clusters with novel transcriptional signatures (Figure 4).

The expression of the 50 sub-cluster-specific DEG (Figure 2D) was analysed in the total lung to determine if they were endothelial specific (Supplementary Figure 4 A). The majority of these DEG were modestly expressed in other cell types. To our knowledge, 39 of 50 identified sub-clusters-specific DEG have not been previously assigned as markers of individual generic subpopulations of BEC in any of the previous studies on human or mouse lung (20, 21, 24, 25, 35). Thus, these 39 DEG novel genes were associated with ageing human lung endothelium. A pathway analysis revealed that they belong to several classes of proteins, including secreted molecules, cell surface receptors and transcription factors, and their sub-cellular distribution (Supplementary Figure 4 B, C).

Ten sub-clusters of ageing human lung BEC had distinct transcriptional signatures, whilst no obvious DEG could be identified for sub-clusters 0 and 5 (Figures 2 B, D, 4A; Supplementary Figure 5). These two sub-clusters had low expression of EC marker genes (Figure 2 C, D), contained a lower average number of genes per cell compared to other BEC

medRxiv preprint doi: https://doi.org/10.1101/2022.03.08.22272025; this version posted March 10, 2022. The copyright holder for this preprint (which was not certified by peer review) is the author/funder, who has granted medRxiv a license to display the preprint in perpetuity.
It is made available under a CC-BY-NC-ND 4.0 International license .

sub-clusters (Supplementary Figure 9 A) and did not express markers of 23 non-EC cell clusters of human lung (Supplementary Table 1; Supplementary Figure 9 B) or stem cells (Supplementary Figure 9 C).

Based on these findings and specific transcriptional signature derived from heatmap analysis (Figure 2 B-D), sub-cluster 0 was annotated as "de-differentiated" BEC. Sub-clusters 1 and 2 were named "bronchial venule 1 (IPF Endo 1)" and "bronchial venule 2 (IPF Endo 2)" BEC. Both clusters had distinct gene expression signatures revealed by heatmaps (Figure 2 B, D) and significant "bronchial" and "vein" identity scores (Figure 2 F; Supplementary Figure 10). "Bronchial venule 1 (IPF Endo 1)" BEC sub-cluster partly, yet non-significantly, matched the "vascular endothelium (VE) peribronchial" sub-cluster signature (Figure 2 F; Supplementary Figure 6) which was identified by others through analysis of age-unmatched datasets of lung tissues from donors and IPF patients (24). Both sub-clusters were annotated "IPF Endo" (1 or 2) due to the increased number of these EC sub-populations in IPF lung (Figure 3). These sub-clusters were differentially present in the two analysed cohorts (Figure 3 A, D), thus intimately linking them to different parts of the lung (the cross-organ region and distal parenchyma in cohorts 2 and 1 respectively, Table 1). Sub-cluster 3 was annotated "general capillary" or "gCap" BEC due to its expression of capillary, and presence of gCap-specific markers *CD36*, *FCN3* and *IL7R* (35); Supplementary Figure 7). Sub-cluster 4 was labelled as "intralobular arteriole" BEC due to its expression of classical arterial differentiation genes (eg. *EFNB2*, *HEY1*, *GJA5*; (41, 42); Supplementary Figure 7, Figure 2F). Sub-cluster 5 was labelled as "de-differentiated capillary" BEC due to either extremely low (*PECAM*, *vWF* and *CLDN5*) or absent (*CDH5* and *CALCRL*) expression levels for general EC markers (Figure 2 C, D), lower average number of genes per cell and lack of expression of specific markers (Supplementary Figure 9 A - C), and a close relationship to general capillary as revealed by pseudo-time lineage analysis (Figure 2 E). Sub-cluster 6 was annotated as "intralobular venule" BEC based on expression of venous differentiation genes (e.g. *NR2F2*, *SOX18* and *TAGLN*; (41, 42); Supplementary Figure 7, Figure 2F). Sub-cluster 7 was labelled as "bronchial capillary" BEC due to its positive scoring for "bronchial" genes signature ((21); Figure 2 F; Supplementary Figure 9), similarity to the "general capillary" BEC sub-cluster (Figure 2 F; Supplementary Figure 7) and high expression of *CD34*, known to be high in lung alveolar capillaries ((43); Figure 2 F; Supplementary Figure 7). Cluster 8 was labelled as "aerocyte" BEC based on its expression of aerocyte-specific markers (*IL1RL1*, *AFF3*, *CA4* and *NCALD*; (35); Figure 2 F; Supplementary Figure 7). Sub-cluster 9 was annotated as "inflammatory" BEC due to high expression of *IL6*, *SELE* and *ICAM1* ((44); Figure 2 D). Sub-cluster 10 was labelled as "de-differentiated venule" BEC based on low expression of pan-EC markers (Figure 2 C, D) and closest proximity to intralobular venule cluster (6) revealed by pseudo-time lineage analysis (Figure 2 E). Sub-cluster 11 was labelled as "de-differentiated arteriole" BEC due to low expression of pan-EC markers (Figure 2 C, D), close proximity to intralobular arteriole sub-cluster (4) revealed by pseudo-time lineage analysis (Figure 2 E) and expression of large vessel markers *NOTCH1*, *HEXB* ((37, 38); Supplementary Figure 7) and *S100A4*, which was also associated with murine and human EC de-differentiation/Endo-MT in *in vitro* models ((36, 39); Supplementary Figure 7). Sub-clusters 10 and 11 were mainly present in cohort 1 (Figure 3 C-E), thus intimately linking their location, and hence origin, to distal parenchyma (Table 1).

Next, we used our novel signatures (Figure 4A) to test the hypothesis that sub-cluster 0 ("de-differentiated" BEC, the largest one in integrated dataset; Figure 3C) is a subpopulation of BEC, which is associated only with ageing and not non-ageing/young human lung. The comparison of an integrated scRNAseq dataset comprising transcriptional profiles of four ageing (49-66 years; donor dataset from cohorts 1; Table 1; (26)) and three non-ageing/young (21-29 years; see Materials and Methods; (26)) human lungs (Supplementary Figure 12) to signatures of ageing human lung BEC sub-populations (Figures 4 A; Supplementary Figure 13 A-B) led to a successful identification of BEC subpopulations in both age groups

medRxiv preprint doi: https://doi.org/10.1101/2022.03.08.22272025; this version posted March 10, 2022. The copyright holder for this preprint (which was not certified by peer review) is the author/funder, who has granted medRxiv a license to display the preprint in perpetuity.
It is made available under a CC-BY-NC-ND 4.0 International license .

(Supplementary Figure 13 C-E), serving as a "proof-of-principle" for the specificity of our novel transcriptional signatures (Supplementary Figure 13 F). All signatures, except for sub-cluster 1 and 2 signatures ("IPF Endo" 1 and 2, which are noticeably associated mainly with ageing IPF lung in cohorts 2 and 1 respectively; Figure 3 B-D), were absent in both age groups (as expected, since these were donor lung samples, Supplementary Figure 13 E). Cell number analysis revealed that BEC sub-cluster zero, which has no obvious DEG, was present only within ageing and not in non-ageing/young human lung (sub-cluster 0, Supplementary Figure 12 B-C; Supplementary Figure 13 E), supporting our hypothesis and its annotation as an ageing-related "de-differentiated" BEC.

Next, unsupervised hierarchical clustering of 12 sub-clusters of ageing human lung BEC from integrated total dataset, which was split into two separate objects (donor and IPF/fibrosis), revealed clear stratification into two groups, which we termed "capillary" (or "microvascular") and "macrovascular", as based on distinct clustering of capillary sub-clusters (3, 5, 7 and 8; Figure 4 D). In IPF, the relationships between sub-clusters were altered, with "bronchial venule 1 (IPF Endo 1)" and "intralobular venule" BEC transcriptional signature "translocating" to "capillary/ microvascular" group (Figure 4 D).

In summary, the conducted comparative analysis and annotation of 12 sub-clusters of ageing human lung BEC led to identification for the first time of 4 sub-clusters of bronchial and 8 sub-clusters of pulmonary circulation, including 4 sub-clusters of "de-differentiated" endothelium. These findings warrant detailed analysis of the roles for these sub-clusters in ageing-associated CLDs.

***Differentially expressed genes analysis and GSEA of the ageing blood vessel endothelium reveal IPF-associated changes in key endothelial cell functions-associated pathways and processes.***

Differential gene expression analysis between donor and IPF for BEC subpopulations led to identification of 3596 significantly regulated (1600 down- and 1996 up-) DEG across 12 sub-clusters (Figure 5 A, B; Supplementary Table 7; Supplementary Figure 14 A). Ingenuity Pathway Analysis (IPA)'s Core expression analysis (45) revealed statistically significant associations of DEG with specific signalling pathways in 7 from 12 sub-clusters (Figure 5 C). DEG from sub-clusters 0, 8 and 11 were directly linked to specific IPF-associated signalling pathways (Figure 5 C, Supplementary Figure 14 B). DEG in four other sub-clusters (1, 2, 3 and 5) were associated with signalling pathways related to fibrotic or inflammatory processes.

Next, the utilisation of published gene set enrichment analysis (GSEA) libraries for the assessment of expression of marker genes, associated with ten EC-relevant cellular or biological processes, revealed significant changes in some ageing human lung BEC subpopulations in IPF (Figure 5 D, E). This included IPF-associated alterations in EC differentiation, mesenchymal, senescence, apoptosis, proliferation, migration, angiogenesis, inflammation , vasodilation and permeability scores, reflecting sub-cluster specific pattern of response to the fibrotic lung environment in all processes, and ranging from two to 8 from total of 9 analysed sub-populations (Supplementary Figure 15).

In summary, our study identified that the balance of EC sub-populations in ageing human lung blood vessel endothelium was significantly changed in IPF, not only in terms of cell numbers, but also DEG, revealing disease-relevant sub-clusters and alterations associated with specific signalling pathways and cellular processes. Changes in transcriptional profiles of individual sub-clusters of ageing human lung BEC related to key endothelial processes suggest implication in clinical manifestations of IPF and sub-cluster-specific functional responses in the fibrotic lung environment.

medRxiv preprint doi: https://doi.org/10.1101/2022.03.08.22272025; this version posted March 10, 2022. The copyright holder for this preprint (which was not certified by peer review) is the author/funder, who has granted medRxiv a license to display the preprint in perpetuity.
It is made available under a CC-BY-NC-ND 4.0 International license .

***Integrated single-cell RNA sequencing analysis reveals heterogeneity of lymphatic endothelial cell population in ageing human lung tissue microenvironment and IPF-associated changes in key endothelial cell functions-associated pathways and processes.***

Finally, to comprehensively decipher the transcriptional signature of ageing human lung lymphatic vessel endothelium in IPF, we extracted scRNAseq data for LEC from the total lung from two cohorts in both conditions (689 cells) and performed unsupervised re-clustering (Figure 1A). This revealed two distinct cell populations of LEC consisting of five subpopulations in total (Supplementary Figure 16 A, B and Supplementary Figure 17). Expression analysis of pan-EC markers and LEC-specific genes (*PROX1*, *PDPN*, *LYVE-1* and *FLT4*) and *CCL21* (Supplementary Figure 16 C) confirmed the identities of all cell subpopulations as LEC. Combined with expression profiles of five genes known to be expressed in LEC (*ACKR2*, *GJA1*, *NFACT1*, *CD34* and *NR2F2*; (29, 46)) and 22 DEG from the heat map (Supplementary Figure 16 D), cell cycle analysis data (Supplementary Figure 16 E, Supplementary Figure 18) and tissue sample collection locations (Table 1), these data formed the basis for the annotation for each of five sub-clusters of LEC (Supplementary Figure 16F). 20 from 22 identified DEG are novel for ageing lung LEC population or its sub-populations (Supplementary Figure 16 F; (21, 25)).

LEC sub-type-specific signatures were generated in a similar manner to BEC sub-clusters analysis (Figure 4 A), using identified DEG and expression of known lymphatic genes (Supplementary Figure 16 G), and were tested for their specificity by comparing cell populations for their similarity to each sub-cluster (Supplementary Figure 16 G and Supplementary Table 8). These signatures were found to be highly specific to their respective sub-clusters, with the exception of signature 2, which also identified cells in sub-clusters zero and 1 (Supplementary Figure 16 H). Quantification of LEC subpopulations revealed no differences between IPF and donor lungs in pooled (Supplementary Figure 19 A and B; Supplementary Table 9) or de-convoluted by cohort (Supplementary Figure 19 C, D and E; Supplementary Table 9) datasets.

Four identified LEC sub-clusters (0, 1, 2 and 4) showed high expression of LEC markers (Supplementary Figure 16 C). Sub-clusters 0 and 2 were annotated as “intralobular lymphatic capillaries” and “subpleural lymphatic capillaries” LEC respectively, based on their high expression of *PDPN*, *LYVE1*, *PROX1* and *FLT4*, linking to findings from studies using other methods (8, 47, 48), and association with specific cohorts, reflecting lung tissue sample collection site (Table 1). Sub-cluster 1 was annotated as “subpleural lymphatic collectors” LEC, as based on their low expression of *LYVE1* and *PROX1* (8, 48). Sub-cluster 4 was identified as “intralobular quiescent para-vascular lymphatics” LEC, as based on high levels of *PDPN* and low levels of *LYVE1* and *PROX1* expression observed for this sub-type of lymphatic vessels (49). For sub-cluster 3, low expression of pan-EC and LEC markers (Supplementary Figure 16 C), close proximity to sub-cluster 4 on UMAP (Supplementary Figure 16 A), high percentage (50.8%) of cells in G2/M phase (Supplementary Figure 16 E) and presence of proliferating EC in para-vascular lymphatics in the IPF lung (49), suggest that it is formed by “proliferating para-vascular lymphatics” LEC. Interestingly, two sub-clusters (1 and 2) originated from cohort 1 and another three (0, 3 and 4) from cohort 2 (Supplementary Figure 19 C-E, Supplementary Table 9). Therefore, annotations matched sample collection locations, with subpleural LEC sub-populations restricted to distal lung samples (Table 1).

Finally, the utilisation of GSEA libraries for the assessment of expression of marker genes associated with ten selected processes relevant to EC biology in LEC subpopulations revealed significant alterations in ageing human lung in IPF (Supplementary Figure 20). These changes indicate sub-cluster specific pattern of response to the fibrotic lung environment in all processes, ranging from zero to three from total of five analysed sub-populations.

medRxiv preprint doi: https://doi.org/10.1101/2022.03.08.22272025; this version posted March 10, 2022. The copyright holder for this preprint (which was not certified by peer review) is the author/funder, who has granted medRxiv a license to display the preprint in perpetuity.
It is made available under a CC-BY-NC-ND 4.0 International license .

In summary, our study is the first to identify five sub-clusters of LEC in ageing human lung. Heterogeneity of LECs was altered in terms of transcriptional profiles and DEG for individual LEC sub-clusters, but without significant alterations in cell numbers. These changes were associated with key endothelial processes, suggesting implication in clinical manifestations of IPF and warranting further investigations for understanding their roles in the fibrotic lung environment and age-associated CLDs.

## DISCUSSION

### *First integrated multi cohort scRNAseq map of age-matched human lungs as a platform for studying endothelium properties and roles in CLDs.*

Ageing is the key risk factor for IPF, although the aetiology of this disease and means of slowing or reversing its progression, remain unclear due to limited understanding of the underlying cellular and molecular mechanisms. Previous studies, aimed at characterising human lung cell heterogeneity and generating cellular atlases, have been predominantly conducted using diverse datasets from healthy donors and patients with different diseases covering a wide range of ages, ethnicities and other characteristics (21, 24-26, 33, 34). This complicated the deconvolution of a highly heterogeneous population of specialised cells in human lung, including changes associated with the ageing process itself or further impacts/exacerbations caused by specific age-associated diseases. For this study, we selected only ageing human lung tissue scRNAseq profiles from two cohorts (24, 26) for integrative analysis, overcoming these limitations and generating a novel map of individual cell populations in age-matched healthy donors and IPF patients.

Unsupervised clustering revealed the presence of 25 distinct cell populations, based on specific gene expression patterns (Figure 1 B, C and Supplementary Figure 2, Supplementary Table 1). Previous studies attempting to characterise changes in transcriptome of the ageing compared to young human lung used bulk RNAseq data, with no comparison to samples from lung diseases in one and inferring cellular composition of the ageing lung in healthy donors and in coronavirus disease-2019 (COVID-19) patients in another (50, 51). A more recent study used human and murine tissues to generate a cell atlas of physiologically ageing and age-matched COPD lungs (20). To our knowledge, the comparative scRNAseq analysis of human lung tissue of elderly IPF patients against age-matched healthy donors has not been conducted. Therefore, the generated in our study integrated multi cohort scRNAseq map of individual cell populations, including endothelium, in age-matched human lung provides a foundation for studying their transcriptional profiles and contribution within respective lung tissue regions and microenvironments in IPF and other age-associated lung diseases.

### *Discovery of previously underappreciated extent of heterogeneity of ageing human lung endothelium.*

Our identification of 17 sub-clusters of EC (12 BEC and 5 LEC) in the ageing human lung with distinct molecular signatures reveals previously underappreciated extent of heterogeneity of ageing human lung endothelium. Herein, we identify 12 sub-clusters of BEC in ageing human lung, with separation of four sub-clusters of bronchial circulation from eight sub-clusters of pulmonary circulation. Previous scRNAseq studies suggested five general and eight specific subpopulations of BEC in human and/or mouse lung (20, 21). Several scRNAseq studies investigated heterogeneity of EC in murine lung tissues, yet to our knowledge only one focused on ageing animals, identifying between five and eight sub-populations (20, 35, 52, 53).

Furthermore, our study identifies 5 sub-clusters of ageing human lung LEC using scRNAseq analysis, matching LEC subpopulations characterised by immunohistochemistry in

medRxiv preprint doi: https://doi.org/10.1101/2022.03.08.22272025; this version posted March 10, 2022. The copyright holder for this preprint (which was not certified by peer review) is the author/funder, who has granted medRxiv a license to display the preprint in perpetuity.
It is made available under a CC-BY-NC-ND 4.0 International license .

human lung (8, 47). To our knowledge, the present study is the first description of distinct molecular signatures of LEC sub-clusters, revealing the heterogeneity of ageing human lung lymphatic endothelium. No studies analysed the transcriptional profile of lymphatic vessel endothelium at a single cell level in the mouse or human lung (from either ageing or young patients), or any other organs, except lymph nodes (54-56). Previously unrecognised heterogeneity of ageing human LEC warrants further study to decipher their role in lung tissue.

DEG signatures for 17 subpopulations of ageing human lung endothelium contain 59 novel candidate genes (39 for BEC and 20 for LEC) for further investigation of their specific roles. A pathway analysis of the DEG (Supplementary Figure 4 B-D) provides a platform for future studies of their, especially cell surface receptors and genes linked to cell metabolism, sub-cluster specific roles in ageing human lung in health and pathophysiology of CLDs.

***De-differentiation and senescence of ageing human lung endothelium and their possible association with vascular and lymphatic function in CLDs.***

Our study identified for the first time the presence of 4 sub-clusters of "de-differentiated" BEC in lungs from ageing human lung (49-72 years old) and their absence in young (21-29 years old) donors. Findings from our scRNAseq analysis in IPF, including expression of transcripts encoding surfactant proteins in some sub-populations, are in accordance with histological and molecular reports about the plasticity of endothelium and loss of EC identity, frequently associated with Endo-MT, in vascular disorders (57-61). In our study, decreases in EC differentiation scores in three BEC sub-clusters (0, 4, 7) and one LEC sub-cluster (0) in IPF co-occurred with increases in mesenchymal score. These findings suggest that Endo-MT is one of the features of the ageing endothelium in IPF, but only in selected BEC and LEC sub-clusters.

Lower average number of genes per cell underlying ageing human lung BEC de-differentiation in sub-clusters zero and five has been also observed in few sub-populations of other cell types within ageing human lung in our study, concordant to findings for individual cell sub-populations identified in scRNAseq studies of ageing tissues from other organs (62, 63). Therefore, this does not appear to be a BEC-specific feature. Sub-clusters zero and five were also negative for other cell type specific markers from the total lung, indicating they are EC and not another cell type. The age-associated de-differentiation of the significant proportion of human lung endothelium sub-populations is the most likely explanation for their "contribution" to sub-cluster zero, which contained nearly 30% of cells within an integrated scRNAseq dataset and manifested as a convergence point for 7 sub-clusters of BEC in ageing human lung tissues samples. The observed down-regulation of EC markers in the ageing human lung could serve as an explanation for immunohistochemistry-based (using CD31, vWF or CD34) reports suggesting a loss of vasculature associated with fibrosis development (9, 64).

Cell cycle analysis revealed that the majority (over 50%) of the cells in sub-clusters zero, four-to-seven and nine in ageing human lung were in S phase. Cell cycle arrest and the increase in S phase proportion have been linked to cell senescence in studies using *in vivo* or *in vitro* models, including murine lung EC (63, 65). All nine analysed ageing human lung BEC sub-populations had positive senescence scores, which increased only in two sub-populations in IPF. Senescence has been classified as a hallmark of ageing in humans and mice (4), but remains challenging to analyse in human tissues and EC within any organ. The presence of senescent endothelium has been associated with hypertension and increased cardiovascular disease risk in elderly patients (66-68). To our knowledge, the cellular senescence in ageing human lung endothelium has not been appreciated at a single cell level before. Therefore, its contribution to alterations in vessel function in lungs of older people under physiological conditions and in CLDs merits further investigation.

medRxiv preprint doi: https://doi.org/10.1101/2022.03.08.22272025; this version posted March 10, 2022. The copyright holder for this preprint (which was not certified by peer review) is the author/funder, who has granted medRxiv a license to display the preprint in perpetuity.
It is made available under a CC-BY-NC-ND 4.0 International license .

De-differentiation (due to Endo MT, global reduction in gene expression and/or partial senescence) of highly specialised EC sub-clusters in ageing human lung is likely to contribute to alterations of function of individual vessel sub-types comprising respective circulatory blood vascular and lymphatic systems. More detailed studies are warranted using tissue samples and *in vitro* models utilising primary lung EC (blood and lymphatic) in order to advance our understanding of the contribution of endothelium de-differentiation in ageing human lung to the pathogenesis and pathophysiology of IPF and other age-associated CLDs.

***Implications of discovering changes in heterogeneity to ageing human lung endothelium in IPF.***

Our study revealed substantial alterations in heterogeneity of ageing human lung endothelium in IPF patients, involving changes in the percentage contribution and transcriptional profiles of individual sub-populations of EC. scRNAseq analysis of ageing human lung showed a significant increase in cell numbers in two ("IPF Endo 1" and "IPF Endo 2") and a decrease in one ("bronchial capillary") BEC sub- populations, and no significant changes in cell numbers in LEC sub-populations in IPF. These novel findings are in accordance with IPF-associated changes in cell numbers for 'VE peribronchial' sub-cluster, which was identified by conducting age-unmatching analysis of lung tissue samples (24). This sub-cluster shares a degree of similarity with two sub-populations of ageing human lung BEC identified in our age-matching study (IPF Endo 1 and 2), that are transcriptionally distinct and derived from two independent cohorts (Figure 2 F), with only one being from the same scRNAseq dataset as 'VE peribronchial' sub-cluster.

Changes in transcriptional profiles of individual sub-clusters of ageing human lung EC related to key endothelial processes suggest an implication in IPF pathophysiology and sub-cluster-specific functional responses in the fibrotic lung environment. Alterations in three BEC sub-clusters from IPF lung included mapping to IPF canonical signalling pathways. This finding suggests a previously unrecognised direct involvement of 'de-differentiated', 'aerocyte' and 'de-differentiated arteriole' BEC from ageing human lung in IPF. Moreover, the association of DEG in other EC sub-clusters from IPF lung with fibrotic signalling (hepatic fibrosis etc.) or inflammatory pathways imply their roles in IPF lung microenvironment. The "IPF Endo 1" sub-cluster translocation from the macrovascular to the capillary/microvascular group in IPF suggests a shift in the transcriptional phenotype of this sub-cluster to a capillary/microvascular-like endothelium, with implied changes to its permeability.

Previous studies of lung vasculature in IPF suggest a contribution of blood vessel dysfunction (16), aberrant angiogenesis (69) and increased permeability of blood vessels to fibrotic lung microenvironment and disease progression (14, 15). Two of the most common co-morbidities in IPF are hypertension and vascular disorders (70, 71), suggesting that there may be systemic as well as lung endothelial dysfunction. Our data suggest that eight BEC sub-clusters show decreases in vasodilation score in IPF compared to the ageing lung with four of these sub-clusters also showing decreases in permeability score in the fibrotic lung. To our knowledge, no functional studies of lymphatic systems and vessel sub-types or LEC composing them performance in ageing human lung or IPF lung have been conducted to date. This warrants further research dissecting the function of the ageing human lung endothelium in IPF, with implications for advancing an understanding of specific roles that individual blood and lymphatic EC subpopulations play in pathophysiology and progression of this disease.

Therapy for IPF patients aims to slow disease progression and maintain lung function (72, 73). The small molecule tyrosine kinase inhibitor drug nintedanib, one of two approved disease-modifying therapies for IPF, acted on *in vitro* cultured human pulmonary microvascular EC to decrease TGF-β2-, TNF-α- and IL-1 β-induced Endo-MT (74). The role of ageing human lung endothelium in the pathogenesis and progression of IPF remains

medRxiv preprint doi: https://doi.org/10.1101/2022.03.08.22272025; this version posted March 10, 2022. The copyright holder for this preprint (which was not certified by peer review) is the author/funder, who has granted medRxiv a license to display the preprint in perpetuity.
It is made available under a CC-BY-NC-ND 4.0 International license .

understudied, partly due to a lack of experimental models which mimic the natural risk factors for this age-associated disease. Understanding of the properties of IPF endothelium and its functions within pre-fibrotic areas and fibrotic lung microenvironment could present new avenues for management of this debilitating and life-threatening disease.

***Summary, conclusions and future perspectives.***

In summary, our study discovered the phenomenon of the distinct "IPF endothelium" phenotype/state, which is based on findings of altered heterogeneity of human ageing lung endothelium from blood and lymphatic vessels in IPF, which contributes to a UIP pattern. We propose that the maintenance of EC heterogeneity, including properties and functions of individual BEC sub-types, in ageing human lung has the potential to improve patients' quality of life, prognosis and protect lung function in IPF. Our molecular findings should help with building a conceptual framework for appreciating the endothelium as a significant contributor within the tissue microenvironments in ageing human lung and a probable target for diagnostics, prognostics and therapy in IPF, other CLDs and diseases associated with fibrosis in other organs, including lymphoedema and cancer.

**ACKNOWLEDGEMENTS.**

We thank all donors who participated in the several studies analysed in this manuscript and the authors who made these rich datasets publicly available. We acknowledge Chris Collins leading support team of the Viper High Performance Computing facility of the University of Hull for their assistance. We thank; Professor Adrian Harris, Professor Tatsuo Shimosawa, Dr. Sarah De Val, Dr. Stephen Henderson, Dr Markus Queisser, Dr. Veronica Carroll, Mr Matthew Morfitt and Mrs Shirin Hasan for their constructive feedback on this manuscript. We specially thank Dr Camille Ettelaie for their contribution towards supporting this research.

**SOURCES OF FUNDING.**

This work was supported by Kate Garthwaite Pulmonary Fibrosis Research Fund, the Endothelial Cell Research Fund and University of Hull PhD Scholarships Fund for "Health Global Data Pipeline (Health*GDP) for biomedical research and clinical applications." cluster.

**DISCLOSURE OF CONFLICTS OF INTEREST.**

None.

## MATERIALS AND METHODS

### Dataset selection

For integrative analysis, lung tissue samples were selected only from age-matched (49-72 years old) donors and IPF patients, and only from those studies that contained samples (cohorts) for both conditions. From all publicly available data sets investigating scRNAseq in IPF and donor lungs (4 in total), only two data sets met this selection criteria representing independent cohorts of subjects/individuals of different ethnic backgrounds. IPF samples and age-matched donor samples in cohort 1 were selected from the gene expression omnibus (GEO) GSE122960_RAW (26) and in cohort 2 - from GSE136831_RAW (24). Only 4 age-matched pairs (scRNAseq data from lung tissue samples from 4 transplantation stage IPF patients and 4 healthy donors) from the cohort 1 (26) matched our selection criteria. Only 5 age-matched pairs from the cohort 2, consisting of 32 IPF and 28 donor samples, ranging from 21 to 80 years old and matching selection criteria (24) were randomly selected for the integrated analysis.

medRxiv preprint doi: https://doi.org/10.1101/2022.03.08.22272025; this version posted March 10, 2022. The copyright holder for this preprint (which was not certified by peer review) is the author/funder, who has granted medRxiv a license to display the preprint in perpetuity.
It is made available under a CC-BY-NC-ND 4.0 International license .

More samples were selected in cohort 2 as they contained less cells per sample than cohort 1. The number of cells analysed per cohort was matched as close as possible. The samples were prepared using overall very similar protocols, but with three differences. Firstly, the samples were collected from peripheral distal lung tissue (parenchyma; 1-2cm) in cohort 1 and from longitudinal sections from apical to basal segments of the lungs in cohort 2. Secondly, cohort 2 samples were processed to derive single cells and then frozen in liquid nitrogen until processed in batches. Samples in cohort 1 were processed as soon as single cells were obtained from tissues. Thirdly, there were variations in reagents for the sample collection processes. The summary of the information on cohort-specific patient characteristics and lung tissue collection sites are outlined in Table 1.

For the analysis of young vs old lung, three samples of young lung (aged 21-29; GSE122960_RAW; (26)) and the healthy elderly donor samples from cohorts 1 and 2 (n=9, aged 49-66, Table 1; GSE122960_RAW, (26); GSE136831_RAW, (24)) were used. The individual samples were given the value 'age' and were labelled as 'young' and 'old' respectively.

**Individual sample processing and quality control.**

Seurat version 4 (v4) was used to perform dimensionality reduction, clustering, and visualization for the scRNAseq data (75). Each individual selected sample was loaded from GEO, and the percentage of mitochondrial genes were calculated for each cell. Cells containing >5000, <200 identified genes or >20% of mitochondrial genes were removed. SCTransform with default parameters was used to normalize and scale the data, and dimensionality reduction was performed using PCA on the top 2000 most variable genes. Each individual sample was processed, and endothelial cells were identified before being saved as an R object before merging all samples into a total Seurat object, performing integration and clustering, as indicated below.

**Dataset integration**

Unique molecular identifiers (UMI) for the remaining after filtering cell barcodes were analysed using the Seurat v4. The UMI counts were normalised using a scale factor of 10,000 UMIs per cell and then natural log transformed using a pseudo count of 1. Integration, embedding and clustering were performed as recommended by Seurat v4 (22). Briefly, the top variable genes within each dataset were selected using the FindVariableFeatures function using the "vst" parameter. Shared patterns of variance in these genes within each dataset where then used to integrate the datasets using Seurat's FindIntegrationAnchors and IntegrateData, then the resulting integrated expression matrix was scaled using Seurat's ScaleData function.

**Dimension reduction, graph embedding, clustering and visualization**

Scaled values from the integrated assay were subject to principal component analysis (PCA). Principal components (PCs) were then subject to feature selection based on ranked contribution to variance. Selected PCs were used to estimate Euclidean distances between cells in feature-space, and cells are graph embedded with edges connecting the nearest neighbours for each cell using the FindNeighbors function. This network of connected cells was then subject to Louvain clustering. The range of possible resolutions to identify these sub-clusters was visualised using clustree R package. Resolution 0.5 was utilised for this analysis and throughput the study. This is comparable to widely used 0.6-0.8 range, which enables avoiding over-clustering (76). For visualization, cell distances and their graph embeddings were subject to uniform manifold approximation and projection (UMAP), where cells are plotted in two-

medRxiv preprint doi: https://doi.org/10.1101/2022.03.08.22272025; this version posted March 10, 2022. The copyright holder for this preprint (which was not certified by peer review) is the author/funder, who has granted medRxiv a license to display the preprint in perpetuity.
It is made available under a CC-BY-NC-ND 4.0 International license .

dimensional feature-space, such that cells with similar transcriptional profiles will appear closer to one another. Further classification of the clusters was preformed using the FindAllMarkers function to identify differentially expressed genes (DEG) between clusters. These DEG were then additionally screened using Violin plots for the expression of these DEG across all clusters.

**Endothelial cell identification**

Following clustering and visualisation of the human aging lung clusters using UMAP, we categorized cell types based on expression profile of classical lineage markers reported by others in the IPF cell atlas covering lung from various ages (21-80) (23). Endothelial cell (EC) cluster was identified using classical (platelet endothelial cell adhesion molecule-1, PECAM1; vascular endothelial cadherin, CDH5; claudin 5, CLDN5) and novel (calcitonin-receptor-like receptor, CLR, encoded by *CALCRL* gene) pan-endothelial markers (29-32, 43). These were further classified into two sub-sets - blood vessel ECs (BEC; based on von Willebrand Factor, vWF, expression) and lymphatic vessel ECs (LEC; based on expression of prospero homeobox 1, PROX1; podoplanin, PDPN; lymphatic vessel endothelial hyaluronan receptor 1, LYVE1 and fms related receptor tyrosine kinase 4, FLT4). Two subsets consisting of only BEC or LEC were created and used for downstream analyses of physiologically aging lungs and IPF lungs from elderly patients. Essential quality controls (filtering data, normalization and endothelial identification; (62)) were conducted for the datasets from individual cohorts (Figure 1A) to confirm comparable quality (uniform reads and presence of clusters of lung cell types in integrated dataset; Supplementary Figure 1; Figure 1B) despite differences in used protocols

**Cluster and sub-cluster screening and profiling**

The data was screened to assess the presence of clusters and sub-clusters containing a low number of genes per cell (62). The number of genes per cell for each cluster in the total lung data was plotted in a violin plot. All of the 25 identified in total ageing human lung clusters were sub-set into their own SeuratObject and were re-clustered to identify sub-clusters. All sub-clusters of the ageing lung were analysed for the number of genes per cell for each cluster. This information was used to confirm if the low number of genes per cell was cell type specific. The expression of a panel of endothelial progenitor markers (*CD34*, *PTPRC*, *KIT*, *POU5F1*, *MYC*, *PROM1*, *CXCR4*, *TEK*, *GYPA*, *NT5E* and *SPN*; (77)) in BEC sub-clusters was also analysed using violin plots.

**Cell trajectory analysis**

We performed a pseudo-time–based cell trajectory analysis using the R package Slingshot (78). The slingshot wrapper function was performed with the UMAP dimensionality reduction and cluster labels as in Seurat objects to identify the trajectory. The subclustered ECs were prepared for processing using the slingshot function as SingleCellExperiment function. The slingshot trajectories are calculated such that each trajectory has a single start and end point. For clarity and brevity, multiple trajectories were plotted on the same graph.

**Cell scoring assay**

The Seurat object for the sub-set BEC and LEC were split using the Seurat SplitObject function by sample condition (donor and fibrosis). The objects were then quired using publicly available transcriptional signatures (GOBP cellular senescence (senescence), Hallmark apoptosis (apoptosis), GOBP endothelial cell proliferation (proliferation), GOBP blood vessel

medRxiv preprint doi: https://doi.org/10.1101/2022.03.08.22272025; this version posted March 10, 2022. The copyright holder for this preprint (which was not certified by peer review) is the author/funder, who has granted medRxiv a license to display the preprint in perpetuity.
It is made available under a CC-BY-NC-ND 4.0 International license .

endothelial cell migration (migration), angiogenesis (angiogenesis), GOBP inflammation (inflammation), GOBP vasodilation (vasodilation) and GOBP regulation of vascular permeability (permeability)) from the GSEA website ((79); http://www.broad.mit.edu/gsea/) developed by the BROAD institute. The libraries for EC differentiation, LEC differentiation and Endo MT were developed from literature. GSEA results should be interpreted as alterations to these processes, not simple increases or decreases as the values may suggest. Therefore, a change in expression of genes outlined in GSEA libraries is termed as a process "score" (s), e.g., EC differentiation or Endo-MT scores etc. The 'scoring' was calculated based on the difference between the average expression levels of the gene set in a particular sub-cluster compared to the total population of cells. "Positive" or "negative" score would suggest that this group (module) of genes is expressed in a particular cell at a higher or lower level respectively, than expected, given the average expression across the cell population. Individual cells were scored using the Seurat function AddModualScore. These scores were then visualised using the Seurat RidgePlot function. A full list of the genes used are summarised in Supplementary Table 8.

**Differential gene expression analysis and Qiagen Ingenuity Pathway Analysis (IPA).**

The Seurat object for the sub-set BEC and LEC were further sub-set so that each cluster became a separate Seurat Object. The active identity of each cluster was then set to sample condition (donor or IPF groups). The Seurat function FindMarkers function was used to identify the differentially expressed genes (DEG) between donor and IPF groups. These genes were then exported into an .xlxs file, along with p-values, logFC and adjusted p-values. This was performed for every sub-cluster. The lists of DEG were uploaded separately into Qiagen IPA software (QIAGEN Inc., https://digitalinsights.qiagen.com/IPA). A core expression analysis was run for each list, taking into account only genes with Wilcoxon rank sum test $P < 0.05$ and querying only human processes. The pathways which had a definitive z score were then summarised in Figure 5 C. IPA's z-score indicates a predicted activation or inhibition of a pathway/gene, where a negative z value connotates an overall pathway's inhibition, and a positive z value connotates an overall pathway's activation.

**Statistical analyses**

Analysis of cell type specific marker genes was performed using the FindAllMarkers function in Seurat v4. This utilises the Wilcoxon rank sum test, with p values adjusted for multiple comparisons using the Bonferroni method. Adjusted p-values of $<0.05$ were considered significant. Significance cell cycle analysis between sample condition was tested using a chi-square test. $P < 0.05$ was considered significant. Analysis of the cell scoring assay was performed using a Shapiro Wilcoxon test to test for normality and Mann-Whitney U test. $P < 0.05$ was considered significant.

**FIGURE LEGENDS.**

**Figure 1. Cell type-specific composition of ageing human lung tissues from donors and IPF patients from two independent cohorts. (A)** Schematic of methodology for samples integration and comprehensive data analysis. Selected data from two studies and grouped into two cohorts (18 samples in total; see Table 1; (24, 26)) were subjected to quality control and merging into an integrated Seurat V4 object for subsequent analysis. Endothelial cell (EC) clusters were identified using pan-endothelial and lymphatic-specific markers. 3192 blood vessel endothelial cells (BEC) and 659 lymphatic vessel endothelial cells (LEC) were identified, and sub-clustered for their characterisation and comparison in donor and IPF

medRxiv preprint doi: https://doi.org/10.1101/2022.03.08.22272025; this version posted March 10, 2022. The copyright holder for this preprint (which was not certified by peer review) is the author/funder, who has granted medRxiv a license to display the preprint in perpetuity.
It is made available under a CC-BY-NC-ND 4.0 International license .

samples. Full details can be found in Materials and Methods. **(B)** UMAP representation of all cells and cell clusters from all 18 samples (pooled). Clusters were numbered and then annotated and labelled according to their detected gene markers. Specific details about each cell population can be found in Supplementary Figure 2 and Supplementary Table 1. Two clusters (LEC and BEC) are labelled with a red circle. **(C, E)** Colour keys for cluster identity is the same as for B. **(C)** Heatmap of top ten differentially expressed genes by the cluster. **(D)** Violin plots and plot_density plots representation of expression data for pan-EC and LEC-specific markers expression in all identified clusters. **(E)** Stacked bar chart of percentage contribution of each cluster to total lung population, split by cohort and condition - donor or fibrosis (IPF). Percent contributions of 3,192 BEC and 659 LEC to the total cell population in ageing human lung are shown with *arrows*. Specific details for each cell population can be found in the Supplementary Table 3. **(F)** UMAP representation of all cells and cell clusters from all 18 samples (pooled), split by condition and labelled by cohort (*blue* – 1; *red* – 2). **(G)** Box and whiskers plot of EC percentage contribution in individual lung samples, split by condition (*blue* – donor; *red* – IPF/fibrosis). Means ± standard deviation (2.501±1.407 for donor and 3.595±2.388 for fibrosis). Statistical analysis was done using Shapiro-Wilk test (p=0.162 for donor and p=0.367 for fibrosis) and unpaired t-test (p = 0.139). (UMAP) Uniform Manifold Approximation and Projection.

**Figure 2. Cell subtype-specific composition of ageing human lung blood vessel endothelial cell cluster from donors and IPF patients from two independent cohorts. (A)** UMAP representation of all cells and cell sub-clusters from original blood vessel endothelial cell (BEC) cluster (from all 18 pooled samples) presented in the Figure 1. Clusters were labelled 0-11 according to their signatures (Supplementary Figure 3), which are presented as **(B)** heatmap of top 10 differentially expressed genes (DEG) by sub-cluster. Specific details about each cell subpopulation can be found in Supplementary Figures 4 and 5, and Supplementary Table 4. All cell clusters can be separated with high confidence (as shown in Supplementary Table 5). **(C)** Violin plots of expression of pan-endothelial and LEC markers in 12 identified BEC sub-clusters. **(D)** Dot plots of genes identified as differentially expressed by the heatmap in B, plotted alongside pan-EC and LEC markers and control genes for comparison, and used in annotation of 12 identified BEC sub-clusters (see also annotation summary presented in Figure 4). **(E)** Representative lineage map in a form of a three-dimensional (3D) UMAP view of 12 identified BEC sub-clusters. Trajectory analysis was performed using the R package Slingshot. Example image from a single angle and additional views and 3D video can be found in Supplementary Figure 6 and Supplementary Video 1. **(F)** Table of module scores (see Materials and Methods) grouped by literature were curated from. CAP1 = Capillary 1, CAP2 = Capillary 2, S Vein = Systemic vein, P Vein = Pulmonary vein, General cap = General capillary. ***Grey*** represents a cluster with negative signature scores in all groups. ***Coral red*** represents a sub-cluster with positive score for signature, colour intensity is proportional the score positivity. Six studies from 2013-2021 include: (i) Gillich et al., 2019 (ii) Vanlandewijck et al., 2019; (iii) Iso et al., 2013; (iv) Nukala et al., 2021; (v) Ochiya et al., 2014; (vi) Herwig et al., 2016. Additional information is available in the main text. (UMAP) Uniform Manifold Approximation and Projection.

**Figure 3. Percentage contributions of blood endothelial cell subpopulations in donors and IPF patients**. **(A)** UMAP of endothelial cells split by sample condition. **(B)** Table detailing the number of cell per cluster, split by condition. **(C-D)** Stacked bar charts of percentage contribution of each cluster to endothelial cell population by sample condition for **(C)** total integrated dataset, **(D)** cohort 1, ***left*** and cohort 2, ***right.*** (UMAP) Uniform Manifold Approximation and Projection.

medRxiv preprint doi: https://doi.org/10.1101/2022.03.08.22272025; this version posted March 10, 2022. The copyright holder for this preprint (which was not certified by peer review) is the author/funder, who has granted medRxiv a license to display the preprint in perpetuity.
It is made available under a CC-BY-NC-ND 4.0 International license .

**Figure 4. Annotation of sub-clusters and relationship between them in donors and IPF patients. (A)** Table summarising the information taken into account for naming/annotating sub-clusters, including gene signatures, sample location by cohort, circulation tree and cell numbers (by condition - donor or IPF/fibrosis). [A] Key colour code for sub-clusters is the same as in Figures 2 and 3. [B] Sample location (by cohort) information corresponds to Table 1. DLP = distal lung parenchyma, LABS = Longitudinal apical to basal segments. [C] Cell number dot plots corresponds to data in Figure 3. **(B)** An example of a histogram (ridgeplot) for the signature 1 in all sub-clusters in both conditions (donor and IPF/fibrosis). Colours are the same as in the [A]Key. **(C)** Table of average module scores of signatures (S1-S11) across all clusters. Signatures 0 and 5 could not be constructed due to a lack of differentially expressed genes (See Figure 2D). See Materials and Methods for full information. **Coral red** intensity represents sub-clusters with a positive module score for signatures. **(D)** Dendrogram (cluster tree) and dot plot of sub-clusters split by condition (donor on the ***left*** and fibrosis on the ***right***).

**Figure 5. Differentially expressed genes linked to specific signalling pathways and cell scoring of gene set enrichment analysis libraries of the ageing blood vessel endothelium reveal changes in IPF.** Differentially expressed genes in individual sub-clusters of blood endothelial cells were analysed and linked to specific signalling pathways. **(A)** An example of volcanoplot of differentially expressed genes (sub-cluster zero). Volcano plots for other clusters can be found in the Supplementary Figure 14. Statistical analysis on normalised data was done using Wilcoxon rank sum test, with p values $P<0.05$ considered significant. **(B)** Doughnut plot of differentially expressed genes between donor and IPF/fibrosis for each sub-cluster. Outer ring shows up-regulated genes and inner ring represents down-regulated genes, with table in the centre showing numbers of differentially expressed genes per cluster. Clusters 9 and 10 were excluded from analysis, as they contained too few cells to analyse between conditions. **(C)** Bar chart detailing the results of the IPA of statistically significant altered pathways. ***Blue colour*** represents a negative Z score (down) and ***orange*** represents a positive Z score (up). DEG from three sub-clusters (4, 6 and 7) did not significantly associate with any pathways and from two others (9 and 10) had too few cells in the IPF group for analysis. Ingenuity pathway analysis (IPA) was performed as described in Materials and Methods. **(D, E)** Published gene set enrichment analysis (GSEA) libraries were utilised for the assessment of expression of marker genes associated with ten selected key/relevant to EC biology processes. Samples were assigned module scores using the Seurat function AddModualScores based on genes used on GSEA website. Please see Materials and Methods section for further details, including scoring and interpretation. Full gene lists are available in Supplementary Table 8. Key colour code for sub-clusters is the same as in Figures 2-4. **(D)** Histograms (ridgeplot) of Endothelial cells differentiation (n= 5), mesenchymal transition (n= 12), inflammation (n= 567), and vasodilation (n= 36) scores in all blood endothelial sub-clusters in donors (***donor***) and IPF (***fibrosis***). Histograms for senescence (n= 79), apoptosis (n= 161), proliferation (n= 54), migration (n= 175), angiogenesis (n= 48), and permeability (n= 40) can be found in Supplementary Figure 15. Number of genes in sets are indicated in brackets. Crucially, histograms show the distribution of a score across sub-cluster (thus reflecting the heterogeneity of gene expression in individual cells within this subpopulation) compared to the total cluster/population. **(E)** Table detailing the p values for difference in module scores between donor and fibrosis. ***Blue colour*** represents a down-regulation and ***orange*** – up-regulation in IPF. Statistical analysis was done using Shapiro Wilcoxon test and Mann-Whitney U test. Black dotted line is added to annotate zero.

medRxiv preprint doi: https://doi.org/10.1101/2022.03.08.22272025; this version posted March 10, 2022. The copyright holder for this preprint (which was not certified by peer review) is the author/funder, who has granted medRxiv a license to display the preprint in perpetuity.
It is made available under a CC-BY-NC-ND 4.0 International license .

**REFERENCES.**

1. Zaman T, Lee JS. Risk factors for the development of idiopathic pulmonary fibrosis: A review. Curr Pulmonol Rep. 2018;7(4):118-25.
2. Maher TM, Bendstrup E, Dron L, Langley J, Smith G, Khalid JM, et al. Global incidence and prevalence of idiopathic pulmonary fibrosis. Respiratory research. 2021;22(1):1-10.
3. Glassberg MK. Overview of idiopathic pulmonary fibrosis, evidence-based guidelines, and recent developments in the treatment landscape. Am J Manag Care. 2019;25(11 Suppl):S195-S203.
4. López-Otín C, Blasco MA, Partridge L, Serrano M, Kroemer G. The hallmarks of aging. Cell. 2013;153(6):1194-217.
5. Strongman H, Kausar I, Maher TM. Incidence, prevalence, and survival of patients with idiopathic pulmonary fibrosis in the UK. Advances in therapy. 2018;35(5):724-36.
6. Wolters PJ, Collard HR, Jones KD. Pathogenesis of idiopathic pulmonary fibrosis. Annu Rev Pathol. 2014;9:157-79.
7. Aspelund A, Robciuc MR, Karaman S, Makinen T, Alitalo K. Lymphatic System in Cardiovascular Medicine. Circ Res. 2016;118(3):515-30.
8. Ebina M, Shibata N, Ohta H, Hisata S, Tamada T, Ono M, et al. The disappearance of subpleural and interlobular lymphatics in idiopathic pulmonary fibrosis. Lymphatic research and biology. 2010;8(4):199-207.
9. Ebina M, Shimizukawa M, Shibata N, Kimura Y, Suzuki T, Endo M, et al. Heterogeneous increase in CD34-positive alveolar capillaries in idiopathic pulmonary fibrosis. American journal of respiratory and critical care medicine. 2004;169(11):1203-8.
10. El-Chemaly S, Malide D, Zudaire E, Ikeda Y, Weinberg BA, Pacheco-Rodriguez G, et al. Abnormal lymphangiogenesis in idiopathic pulmonary fibrosis with insights into cellular and molecular mechanisms. Proc Natl Acad Sci U S A. 2009;106(10):3958-63.
11. Gaje PN, Stoia-Djeska I, Cimpean AM, Ceausu RA, Tudorache V, Raica M. Lymphangiogenesis as a Prerequisite in the Pathogenesis of Lung Fibrosis. in vivo. 2014;28(3):367-73.
12. Glasgow CG, El-Chemaly S, Moss J. Lymphatics in lymphangioleiomyomatosis and idiopathic pulmonary fibrosis. European Respiratory Review. 2012;21(125):196-206.
13. Lara AR, Cosgrove GP, Janssen WJ, Huie TJ, Burnham EL, Heinz DE, et al. Increased lymphatic vessel length is associated with the fibroblast reticulum and disease severity in usual interstitial pneumonia and nonspecific interstitial pneumonia. Chest. 2012;142(6):1569-76.
14. Montesi SB, Rao R, Liang LL, Goulart HE, Sharma A, Digumarthy SR, et al. Gadofosveset-enhanced lung magnetic resonance imaging to detect ongoing vascular leak in pulmonary fibrosis. European Respiratory Journal. 2018;51(5).
15. Montesi SB, Zhou IY, Liang LL, Digumarthy SR, Mercaldo S, Mercaldo N, et al. Dynamic contrast-enhanced magnetic resonance imaging of the lung reveals important pathobiology in idiopathic pulmonary fibrosis. ERJ open research. 2021;7(4).
16. Probst CK, Montesi SB, Medoff BD, Shea BS, Knipe RS. Vascular permeability in the fibrotic lung. European Respiratory Journal. 2020;56(1).
17. Sgalla G, Iovene B, Calvello M, Ori M, Varone F, Richeldi L. Idiopathic pulmonary fibrosis: pathogenesis and management. Respiratory research. 2018;19(1):1-18.
18. Sharara RS, Hattab Y, Patel K, DiSilvio B, Singh AC, Malik K. Introduction to the anatomy and physiology of pulmonary circulation. Critical Care Nursing Quarterly. 2017;40(3):181-90.
19. Stump B, Cui Y, Kidambi P, Lamattina AM, El-Chemaly S. Lymphatic Changes in Respiratory Diseases: More than Just Remodeling of the Lung? Am J Respir Cell Mol Biol. 2017;57(3):272-9.

medRxiv preprint doi: https://doi.org/10.1101/2022.03.08.22272025; this version posted March 10, 2022. The copyright holder for this preprint (which was not certified by peer review) is the author/funder, who has granted medRxiv a license to display the preprint in perpetuity.
It is made available under a CC-BY-NC-ND 4.0 International license .

20. Sauler M, McDonough JE, Adams TS, Kothapalli N, Barnthaler T, Werder RB, et al. Characterization of the COPD alveolar niche using single-cell RNA sequencing. Nature Communications. 2022;13(1):1-17.
21. Travaglini KJ, Nabhan AN, Penland L, Sinha R, Gillich A, Sit RV, et al. A molecular cell atlas of the human lung from single-cell RNA sequencing. Nature. 2020;587(7835):619-25.
22. Stuart T, Satija R. Integrative single-cell analysis. Nat Rev Genet. 2019;20(5):257-72.
23. Neumark N, Cosme Jr C, Rose K-A, Kaminski N. The idiopathic pulmonary fibrosis cell atlas. American Physiological Society Bethesda, MD; 2020. p. L887-L92.
24. Adams TS, Schupp JC, Poli S, Ayaub EA, Neumark N, Ahangari F, et al. Single-cell RNA-seq reveals ectopic and aberrant lung-resident cell populations in idiopathic pulmonary fibrosis. Science advances. 2020;6(28):eaba1983.
25. Schupp JC, Adams TS, Cosme Jr C, Raredon MSB, Yuan Y, Omote N, et al. Integrated single-cell atlas of endothelial cells of the human lung. Circulation. 2021;144(4):286-302.
26. Reyfman PA, Walter JM, Joshi N, Anekalla KR, McQuattie-Pimentel AC, Chiu S, et al. Single-cell transcriptomic analysis of human lung provides insights into the pathobiology of pulmonary fibrosis. American journal of respiratory and critical care medicine. 2019;199(12):1517-36.
27. Morse C, Tabib T, Sembrat J, Buschur KL, Bittar HT, Valenzi E, et al. Proliferating SPP1/MERTK-expressing macrophages in idiopathic pulmonary fibrosis. European Respiratory Journal. 2019;54(2).
28. He D, Wang D, Lu P, Yang N, Xue Z, Zhu X, et al. Single-cell RNA sequencing reveals heterogeneous tumor and immune cell populations in early-stage lung adenocarcinomas harboring EGFR mutations. Oncogene. 2021;40(2):355-68.
29. Johnson NC, Dillard ME, Baluk P, McDonald DM, Harvey NL, Frase SL, et al. Lymphatic endothelial cell identity is reversible and its maintenance requires Prox1 activity. Genes & development. 2008;22(23):3282-91.
30. Müller AM, Hermanns MI, Skrzynski C, Nesslinger M, Müller KM, Kirkpatrick CJ. Expression of the endothelial markers PECAM-1, vWf, and CD34 in vivo and in vitro. Exp Mol Pathol. 2002;72(3):221-9.
31. Nikitenko LL, Smith DM, Bicknell R, Rees MC. Transcriptional regulation of the CRLR gene in human microvascular endothelial cells by hypoxia. The FASEB journal. 2003;17(11):1-25.
32. Wigle JT, Harvey N, Detmar M, Lagutina I, Grosveld G, Gunn MD, et al. An essential role for Prox1 in the induction of the lymphatic endothelial cell phenotype. Embo j. 2002;21(7):1505-13.
33. Habermann AC, Gutierrez AJ, Bui LT, Yahn SL, Winters NI, Calvi CL, et al. Single-cell RNA sequencing reveals profibrotic roles of distinct epithelial and mesenchymal lineages in pulmonary fibrosis. Science advances. 2020;6(28):eaba1972.
34. Vieira Braga FA, Kar G, Berg M, Carpaij OA, Polanski K, Simon LM, et al. A cellular census of human lungs identifies novel cell states in health and in asthma. Nat Med. 2019;25(7):1153-63.
35. Gillich A, Zhang F, Farmer CG, Travaglini KJ, Tan SY, Gu M, et al. Capillary cell-type specialization in the alveolus. Nature. 2020;586(7831):785-9.
36. Herwig N, Belter B, Pietzsch J. Extracellular S100A4 affects endothelial cell integrity and stimulates transmigration of A375 melanoma cells. Biochemical and Biophysical Research Communications. 2016;477(4):963-9.
37. Iso T, Kedes L, Hamamori Y. HES and HERP families: multiple effectors of the Notch signaling pathway. J Cell Physiol. 2003;194(3):237-55.
38. Nukala SB, Tura-Ceide O, Aldini G, Smolders V, Blanco I, Peinado VI, et al. Protein network analyses of pulmonary endothelial cells in chronic thromboembolic pulmonary hypertension. Sci Rep. 2021;11(1):5583.

medRxiv preprint doi: https://doi.org/10.1101/2022.03.08.22272025; this version posted March 10, 2022. The copyright holder for this preprint (which was not certified by peer review) is the author/funder, who has granted medRxiv a license to display the preprint in perpetuity.
It is made available under a CC-BY-NC-ND 4.0 International license .

39. Ochiya T, Takenaga K, Endo H. Silencing of S100A4, a metastasis-associated protein, in endothelial cells inhibits tumor angiogenesis and growth. Angiogenesis. 2014;17(1):17-26.
40. Vanlandewijck M, He L, Mäe MA, Andrae J, Ando K, Del Gaudio F, et al. A molecular atlas of cell types and zonation in the brain vasculature. Nature. 2018;554(7693):475-80.
41. Adams RH. Molecular control of arterial–venous blood vessel identity. Journal of Anatomy. 2003;202(1):105-12.
42. Swift MR, Weinstein BM. Arterial-venous specification during development. Circ Res. 2009;104(5):576-88.
43. Pusztaszeri MP, Seelentag W, Bosman FT. Immunohistochemical expression of endothelial markers CD31, CD34, von Willebrand factor, and Fli-1 in normal human tissues. J Histochem Cytochem. 2006;54(4):385-95.
44. Pober JS, Sessa WC. Evolving functions of endothelial cells in inflammation. Nature Reviews Immunology. 2007;7(10):803-15.
45. Krämer A, Green J, Pollard Jr J, Tugendreich S. Causal analysis approaches in ingenuity pathway analysis. Bioinformatics. 2014;30(4):523-30.
46. Fiedler U, Augustin HG. Angiopoietins: a link between angiogenesis and inflammation. Trends Immunol. 2006;27(12):552-8.
47. Kambouchner M, Bernaudin J-F. Intralobular pulmonary lymphatic distribution in normal human lung using D2-40 antipodoplanin immunostaining. Journal of Histochemistry & Cytochemistry. 2009;57(7):643-8.
48. Mori M, Andersson CK, Graham GJ, Löfdahl C-G, Erjefält JS. Increased number and altered phenotype of lymphatic vessels in peripheral lung compartments of patients with COPD. Respiratory research. 2013;14(1):1-19.
49. Baluk P, Naikawadi RP, Kim S, Rodriguez F, Choi D, Hong YK, et al. Lymphatic Proliferation Ameliorates Pulmonary Fibrosis after Lung Injury. Am J Pathol. 2020;190(12):2355-75.
50. Chow RD, Majety M, Chen S. The aging transcriptome and cellular landscape of the human lung in relation to SARS-CoV-2. Nature Communications. 2021;12(1):1-13.
51. Lee S, Islam MN, Boostanpour K, Aran D, Jin G, Christenson S, et al. Molecular programs of fibrotic change in aging human lung. Nature communications. 2021;12(1):1-10.
52. Kalucka J, de Rooij LP, Goveia J, Rohlenova K, Dumas SJ, Meta E, et al. Single-cell transcriptome atlas of murine endothelial cells. Cell. 2020;180(4):764-79. e20.
53. Niethamer TK, Stabler CT, Leach JP, Zepp JA, Morley MP, Babu A, et al. Defining the role of pulmonary endothelial cell heterogeneity in the response to acute lung injury. Elife. 2020;9:e53072.
54. Sibler E, He Y, Ducoli L, Keller N, Fujimoto N, Dieterich LC, et al. Single-cell transcriptional heterogeneity of lymphatic endothelial cells in normal and inflamed murine lymph nodes. Cells. 2021;10(6):1371.
55. Takeda A, Hollmén M, Dermadi D, Pan J, Brulois KF, Kaukonen R, et al. Single-Cell Survey of Human Lymphatics Unveils Marked Endothelial Cell Heterogeneity and Mechanisms of Homing for Neutrophils. Immunity. 2019;51(3):561-72.e5.
56. Xiang M, Grosso RA, Takeda A, Pan J, Bekkhus T, Brulois K, et al. A Single-Cell Transcriptional Roadmap of the Mouse and Human Lymph Node Lymphatic Vasculature. Front Cardiovasc Med. 2020;7:52.
57. Bhatti F, Ball G, Hobbs R, Linens A, Munzar S, Akram R, et al. Pulmonary surfactant protein a is expressed in mouse retina by Müller cells and impacts neovascularization in oxygen-induced retinopathy. Invest Ophthalmol Vis Sci. 2014;56(1):232-42.
58. Colmorten KB, Nexoe AB, Sorensen GL. The Dual Role of Surfactant Protein-D in Vascular Inflammation and Development of Cardiovascular Disease. Front Immunol. 2019;10:2264.
59. Dejana E, Hirschi KK, Simons M. The molecular basis of endothelial cell plasticity. Nat Commun. 2017;8:14361.

medRxiv preprint doi: https://doi.org/10.1101/2022.03.08.22272025; this version posted March 10, 2022. The copyright holder for this preprint (which was not certified by peer review) is the author/funder, who has granted medRxiv a license to display the preprint in perpetuity.
It is made available under a CC-BY-NC-ND 4.0 International license .

60. Gaikwad AV, Eapen MS, McAlinden KD, Chia C, Larby J, Myers S, et al. Endothelial to mesenchymal transition (EndMT) and vascular remodeling in pulmonary hypertension and idiopathic pulmonary fibrosis. Expert Review of Respiratory Medicine. 2020;14(10):1027-43.
61. Piera-Velazquez S, Mendoza FA, Jimenez SA. Endothelial to mesenchymal transition (EndoMT) in the pathogenesis of human fibrotic diseases. Journal of clinical medicine. 2016;5(4):45.
62. Durante MA, Kurtenbach S, Sargi ZB, Harbour JW, Choi R, Kurtenbach S, et al. Single-cell analysis of olfactory neurogenesis and differentiation in adult humans. Nat Neurosci. 2020;23(3):323-6.
63. Kumari R, Jat P. Mechanisms of cellular senescence: cell cycle arrest and senescence associated secretory phenotype. Frontiers in cell and developmental biology. 2021;9:485.
64. Barratt S, Millar A. Vascular remodelling in the pathogenesis of idiopathic pulmonary fibrosis. QJM: An International Journal of Medicine. 2014;107(7):515-9.
65. van Deursen JM. The role of senescent cells in ageing. Nature. 2014;509(7501):439-46.
66. Minamino T, Miyauchi H, Yoshida T, Ishida Y, Yoshida H, Komuro I. Endothelial cell senescence in human atherosclerosis: role of telomere in endothelial dysfunction. Circulation. 2002;105(13):1541-4.
67. Seals DR, Jablonski KL, Donato AJ. Aging and vascular endothelial function in humans. Clin Sci (Lond). 2011;120(9):357-75.
68. Versari D, Daghini E, Virdis A, Ghiadoni L, Taddei S. The ageing endothelium, cardiovascular risk and disease in man. Exp Physiol. 2009;94(3):317-21.
69. Barratt SL, Creamer A, Hayton C, Chaudhuri N. Idiopathic pulmonary fibrosis (IPF): an overview. Journal of clinical medicine. 2018;7(8):201.
70. Farkas L, Gauldie J, Voelkel NF, Kolb M. Pulmonary hypertension and idiopathic pulmonary fibrosis: a tale of angiogenesis, apoptosis, and growth factors. Am J Respir Cell Mol Biol. 2011;45(1):1-15.
71. Hubbard RB, Smith C, Le Jeune I, Gribbin J, Fogarty AW. The association between idiopathic pulmonary fibrosis and vascular disease: a population-based study. Am J Respir Crit Care Med. 2008;178(12):1257-61.
72. Maher TM, Strek ME. Antifibrotic therapy for idiopathic pulmonary fibrosis: time to treat. Respir Res. 2019;20(1):205.
73. Raghu G, Rochwerg B, Zhang Y, Garcia CA, Azuma A, Behr J, et al. An Official ATS/ERS/JRS/ALAT Clinical Practice Guideline: Treatment of Idiopathic Pulmonary Fibrosis. An Update of the 2011 Clinical Practice Guideline. Am J Respir Crit Care Med. 2015;192(2):e3-19.
74. Tsutsumi T, Nagaoka T, Yoshida T, Wang L, Kuriyama S, Suzuki Y, et al. Nintedanib ameliorates experimental pulmonary arterial hypertension via inhibition of endothelial mesenchymal transition and smooth muscle cell proliferation. PLoS One. 2019;14(7):e0214697.
75. Hao Y, Hao S, Andersen-Nissen E, Mauck W, Zheng S, Butler A, et al. Integrated analysis of multimodal single-cell data. bioRxiv; 2020.
76. Luecken MD, Theis FJ. Current best practices in single-cell RNA-seq analysis: a tutorial. Mol Syst Biol. 2019;15(6):e8746.
77. Hristov M, Erl W, Weber PC. Endothelial progenitor cells: mobilization, differentiation, and homing. Arterioscler Thromb Vasc Biol. 2003;23(7):1185-9.
78. Street K, Risso D, Fletcher RB, Das D, Ngai J, Yosef N, et al. Slingshot: cell lineage and pseudotime inference for single-cell transcriptomics. BMC genomics. 2018;19(1):1-16.
79. Subramanian A, Tamayo P, Mootha VK, Mukherjee S, Ebert BL, Gillette MA, et al. Gene set enrichment analysis: a knowledge-based approach for interpreting genome-wide expression profiles. Proc Natl Acad Sci U S A. 2005;102(43):15545-50.

medRxiv preprint doi: https://doi.org/10.1101/2022.03.08.22272025; this version posted March 10, 2022. The copyright holder for this preprint **(which was not certified by peer review)** is the author/funder, who has granted medRxiv a license to display the preprint in perpetuity.
It is made available under a CC-BY-NC-ND 4.0 International license .

# TABLES

**Table 1. Characteristics of ageing human lung tissue samples split by cohort.**
Cohort 1 (8 samples) was from GSE122960_RAW (Reyfman et al., 2019) and cohort 2 (10 samples) was from GSE136831 (Adams et al., 2020). M = male, F = female, IPF = idiopathic pulmonary fibrosis, N/A = not applicable.

**Cohort 1**

| Sample ID | Age (yr) | Sex | Race | Diagnosis | Sample location | Number of cells |
|---|---|---|---|---|---|---|
| D1 | 63 | F | African american | N/A | 1-2 cm distal lung parenchyma | 6951 |
| D2 | 55 | M | Asian | N/A | | 6625 |
| D4 | 57 | F | African american | N/A | | 9843 |
| D5 | 49 | F | White | N/A | | 9108 |
| IPF 1 | 66 | M | Unknown | IPF | 1-2 cm distal lung parenchyma | 4872 |
| IPF 2 | 60 | M | Unknown | IPF | | 3670 |
| IPF 3 | 68 | M | Unknown | IPF | | 11035 |
| IPF 4 | 72 | F | Unknown | IPF | | 5940 |

**Cohort 2**

| Sample ID | Age (yr) | Sex | Race | Diagnosis | Sample location | Number of cells |
|---|---|---|---|---|---|---|
| 439C | 66 | F | White | N/A | Longitudinal biopsies from apical to most basal segments of the lung | 9198 |
| 065C | 66 | F | White | N/A | | 2403 |
| 388C | 61 | M | White | N/A | | 3088 |
| 192C | 62 | F | White | N/A | | 5002 |
| 160C | 64 | M | White | N/A | | 3981 |
| 221I | 67 | M | White | IPF | Longitudinal biopsies from apical to most basal segments of the lung | 6931 |
| 222I | 59 | M | White | IPF | | 10354 |
| 021I | 69 | M | White | IPF | | 4090 |
| 29I | 61 | M | White | IPF | | 1335 |
| 0631I-b | 68 | M | White | IPF | | 4419 |

medRxiv preprint doi: https://doi.org/10.1101/2022.03.08.22272025; this version posted March 10, 2022. The copyright holder for this preprint (which was not certified by peer review) is the author/funder, who has granted medRxiv a license to display the preprint in perpetuity.
It is made available under a CC-BY-NC-ND 4.0 International license .

# FIGURE 1

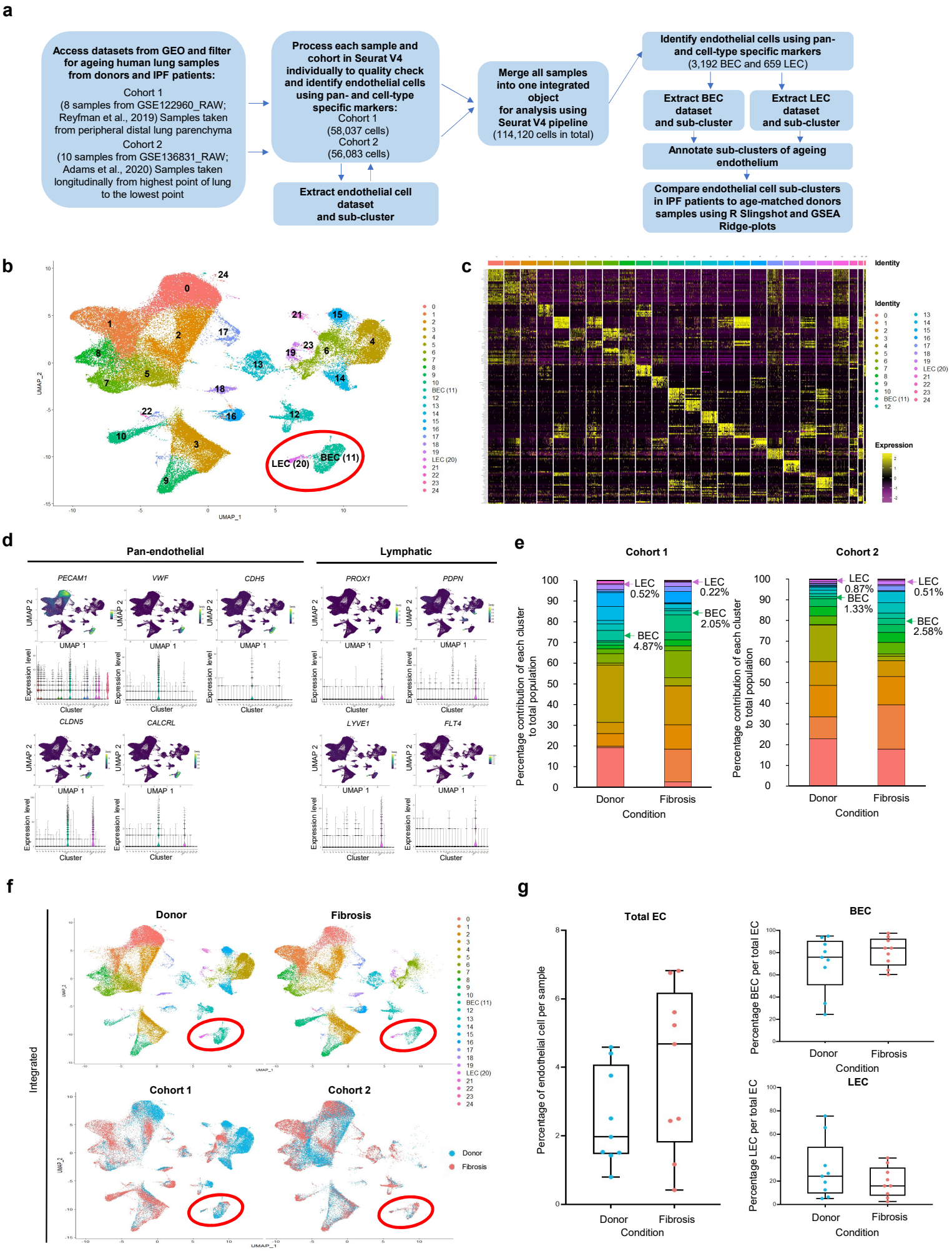

medRxiv preprint doi: https://doi.org/10.1101/2022.03.08.22272025; this version posted March 10, 2022. The copyright holder for this preprint **(which was not certified by peer review)** is the author/funder, who has granted medRxiv a license to display the preprint in perpetuity.
It is made available under a CC-BY-NC-ND 4.0 International license .

# FIGURE 2

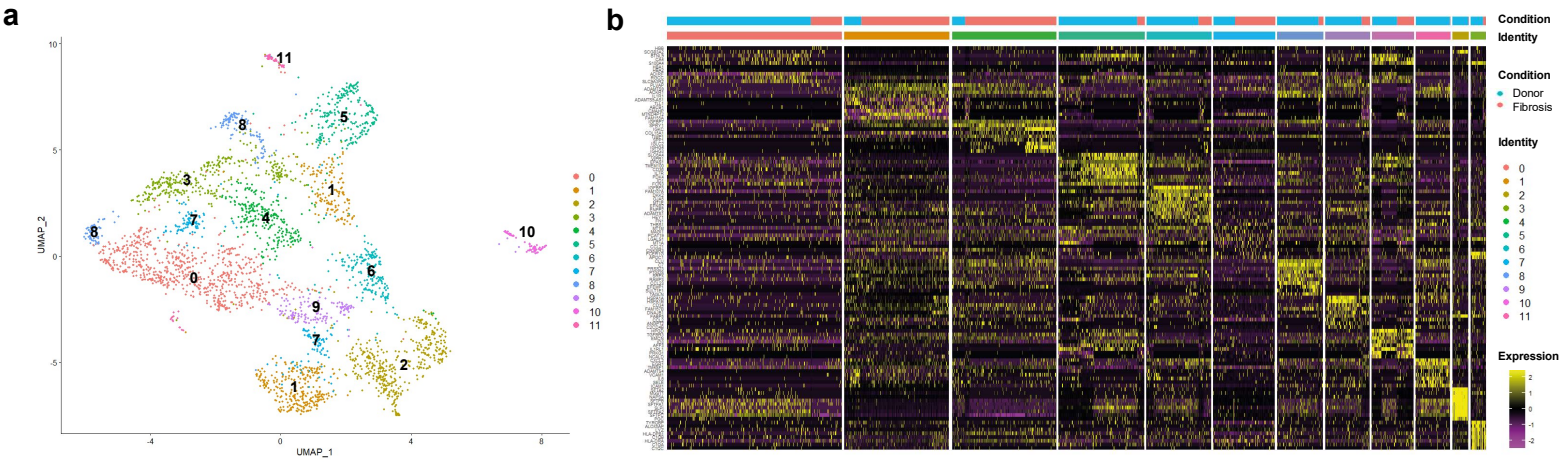


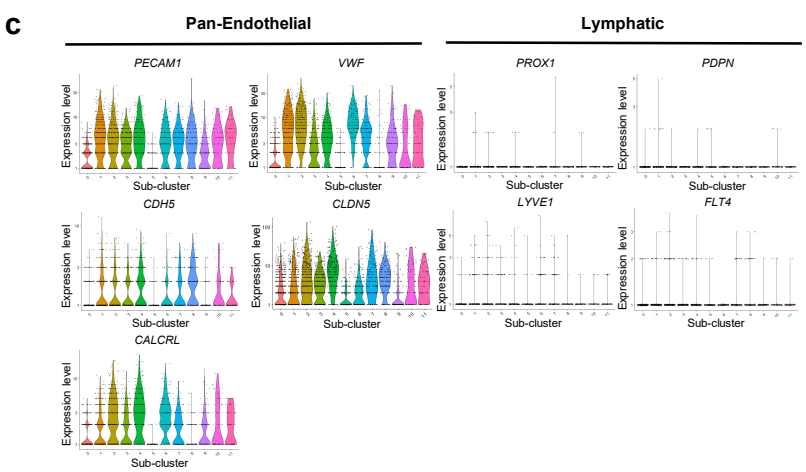


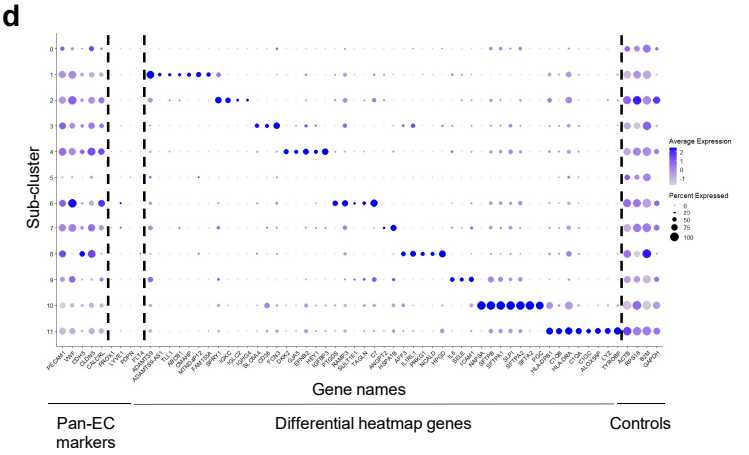


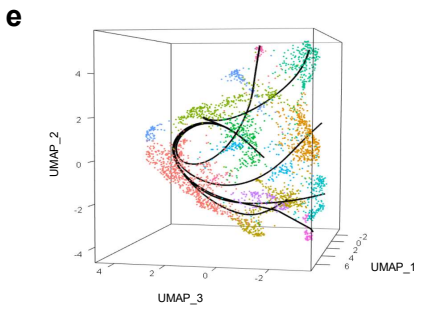


f

| BEC sub-cluster | Signatures | | | | | | | | | | | | | | | | | | | | | | | | |
|---|---|---|---|---|---|---|---|---|---|---|---|---|---|---|---|---|---|---|---|---|---|---|---|---|---|
| | Seven studies 2013-2021 | | | | | Travagliniet al., 2020 | | | | | Adams et al., 2020 | | | | | Schupp et al., 2021 | | | | | Sauler et al., 2022 | | | | |
| | Artery | Vein | gCAP | aCAP | Large | Art | Vein | CAP1 | CAP2 | Bronc | Artery | Vein | Capillary A | Capillary B | Peribronchial | Artery | S vein | Pvein | Acap | Gcap | Artery | Vein | aCAP | gCAP | PeriB |
| 0 | -0.045 | 0.024 | -0.234 | 0.185 | 0.103 | 0.018 | -0.148 | 0.231 | -0.197 | -0.123 | -0.003 | -0.053 | 0.045 | 0.081 | -0.156 | 0.001 | -0.102 | -0.081 | 0.123 | 0.043 | -0.070 | -0.051 | 0.163 | 0.736 | -0.179 |
| 1 | -0.104 | -0.113 | -0.368 | -0.173 | -0.099 | -0.189 | 0.586 | -0.170 | -0.591 | -0.035 | -0.069 | -0.164 | -0.151 | -0.276 | 0.635 | -0.103 | 0.151 | -0.014 | -0.193 | -0.349 | -0.218 | 0.302 | -0.612 | -0.054 | 0.066 |
| 2 | -0.144 | 0.196 | -0.511 | -0.194 | -0.038 | -0.139 | 0.878 | -0.066 | -0.631 | 0.372 | -0.115 | -0.023 | -0.190 | -0.172 | 0.549 | -0.085 | 0.226 | 0.162 | -0.162 | -0.380 | -0.323 | 0.383 | -0.639 | -0.077 | 0.280 |
| 3 | 0.001 | -0.093 | 0.689 | 0.004 | 0.061 | -0.057 | -0.287 | -0.039 | 0.869 | -0.389 | -0.065 | -0.238 | 0.170 | 0.700 | -0.294 | -0.050 | -0.293 | -0.276 | -0.015 | 0.807 | -0.266 | -0.160 | 0.166 | 1.967 | -0.344 |
| 4 | 0.495 | -0.046 | -0.468 | -0.182 | -0.054 | 0.884 | -0.434 | -0.105 | -0.544 | -0.131 | 0.559 | -0.071 | -0.272 | 0.039 | -0.409 | 0.583 | -0.312 | -0.139 | -0.183 | -0.274 | 0.912 | -0.249 | -0.634 | 0.513 | -0.338 |
| 5 | -0.035 | -0.055 | -0.015 | 0.012 | 0.083 | -0.064 | 0.159 | 0.047 | -0.100 | -0.105 | -0.043 | -0.115 | -0.008 | -0.042 | 0.080 | -0.039 | -0.050 | -0.053 | 0.033 | 0.010 | -0.134 | -0.034 | -0.127 | 0.249 | -0.102 |
| 6 | -0.163 | 1.057 | -0.113 | -0.185 | 0.002 | -0.119 | 1.379 | -0.102 | -0.079 | 0.080 | 0.043 | 0.636 | -0.208 | 0.404 | 0.163 | -0.088 | -0.117 | 0.789 | -0.142 | -0.089 | -0.319 | 0.776 | -0.551 | 0.937 | -0.182 |
| 7 | -0.116 | -0.027 | -0.390 | -0.055 | 0.028 | -0.159 | 0.275 | 0.004 | -0.491 | 0.123 | -0.099 | -0.127 | -0.164 | -0.050 | 0.221 | -0.071 | -0.016 | -0.108 | -0.114 | -0.148 | -0.215 | 0.112 | -0.429 | 0.307 | 0.089 |
| 8 | -0.163 | -0.195 | -0.166 | 1.013 | 0.283 | -0.131 | -0.364 | 0.856 | -0.207 | -0.393 | -0.145 | -0.176 | 0.827 | -0.023 | -0.418 | -0.139 | -0.263 | -0.229 | 0.887 | -0.103 | -0.292 | -0.260 | 1.503 | 0.652 | -0.405 |
| 9 | -0.116 | 0.414 | -0.406 | -0.121 | 0.271 | -0.126 | 1.091 | -0.101 | -0.390 | 0.251 | 0.048 | 0.377 | -0.200 | -0.067 | 0.491 | -0.054 | 0.036 | 0.527 | -0.135 | -0.256 | -0.233 | 0.867 | -0.459 | 0.323 | -0.085 |
| 10 | -0.130 | -0.152 | -0.609 | -0.078 | -0.014 | -0.098 | -0.531 | 0.004 | -0.578 | -0.275 | -0.074 | -0.257 | -0.237 | -0.442 | -0.426 | -0.052 | -0.296 | -0.195 | -0.086 | -0.270 | -0.218 | -0.287 | -0.473 | -0.009 | -0.470 |
| 11 | -0.140 | -0.163 | -0.307 | -0.155 | 0.373 | -0.059 | -0.170 | -0.118 | -0.382 | -0.280 | -0.094 | -0.202 | -0.198 | -0.226 | -0.297 | -0.116 | -0.225 | -0.215 | 0.064 | -0.162 | -0.194 | -0.167 | -0.379 | 0.208 | -0.377 |

medRxiv preprint doi: https://doi.org/10.1101/2022.03.08.22272025; this version posted March 10, 2022. The copyright holder for this preprint **(which was not certified by peer review)** is the author/funder, who has granted medRxiv a license to display the preprint in perpetuity.
It is made available under a CC-BY-NC-ND 4.0 International license .

# FIGURE 3

**a**

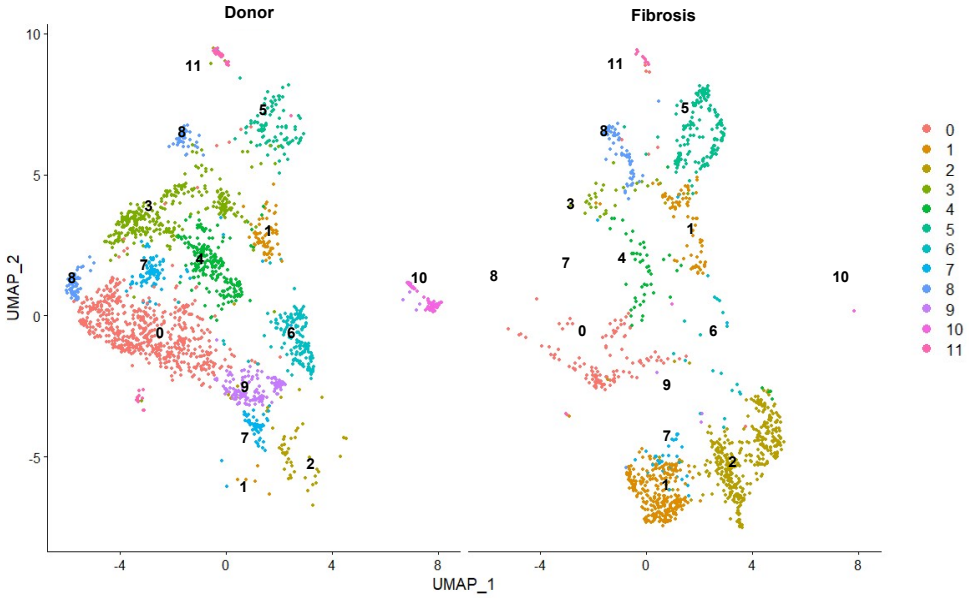


**b**

| BEC sub-cluster | Cell numbers, n (%) | |
|---|---|---|
| | Donor | Fibrosis |
| 0 | 577 (29.3) | 124 (10.1) |
| 1 | 70 (3.5) | 352 (28.8) |
| 2 | 51 (2.6) | 367 (30) |
| 3 | 316 (16) | 29 (2.4) |
| 4 | 209 (10.6) | 51 (4.2) |
| 5 | 87 (4.4) | 161 (13.2) |
| 6 | 166 (8.4) | 19 (1.6) |
| 7 | 145 (7.4) | 34 (2.8) |
| 8 | 100 (5.1) | 68 (5.6) |
| 9 | 136 (6.9) | 3 (0.3) |
| 10 | 63 (3.2) | 2 (0.2) |
| 11 | 50 (2.5) | 12 (1) |

**c**

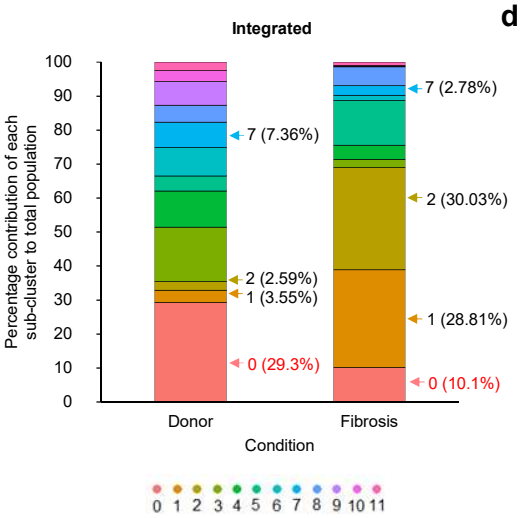


**d**

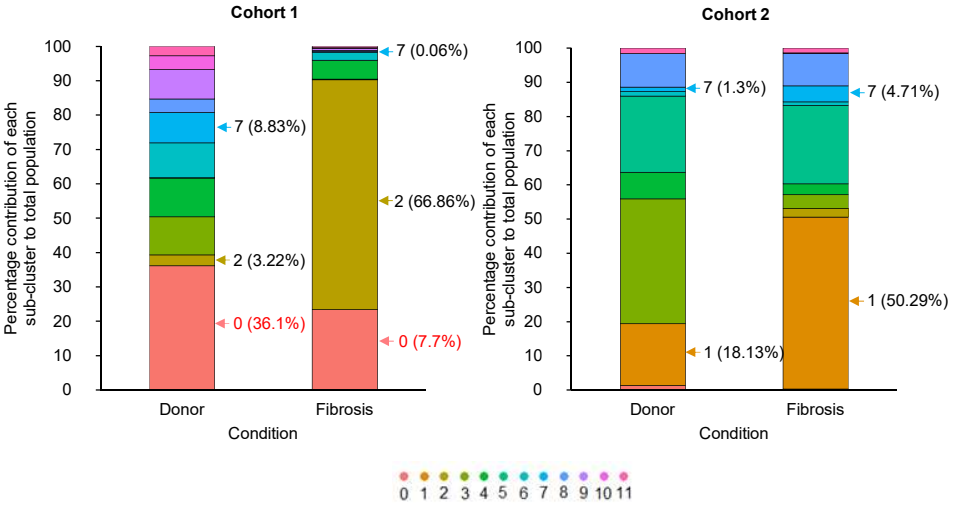

medRxiv preprint doi: https://doi.org/10.1101/2022.03.08.22272025; this version posted March 10, 2022. The copyright holder for this preprint **(which was not certified by peer review)** is the author/funder, who has granted medRxiv a license to display the preprint in perpetuity.
It is made available under a CC-BY-NC-ND 4.0 International license .

# FIGURE 4

**a**

| BEC sub-cluster | | | | Cohort (location)[b] | | Circulation | | Cell numbers[c] (100 200 300 400 500) | |
|---|---|---|---|---|---|---|---|---|---|
| KEY[a] | Number | Annotation | Genes | DLP | LABS | Broncial | Pulmonary | Donor | Fibrosis |
| | 0 | De-differentiated | Negativity for all markers and low expression of pan-endothelial EC markers | | | | | ● | • |
| | 1 | Bronchial venule (IPF Endo 1) | *ADAMTS9, ADAMTS9-AS1, TLL1, ABCB1, CMAHP, MTND412, FAM155A* | | | | | • | ● |
| | 2 | Bronchial venule (IPF Endo 2) | *SPRY1, IGCK, IGLC2, IGHG4* | | | | | · | ● |
| | 3 | General capillary (gCAP) | *SLC6A4, CD36, FCN3* | | | | | ● | • |
| | 4 | Intralobular arteriole | *DKK2, GJA5, EFNB2, HEY1, IGFBP3* | | | | | • | • |
| | 5 | De-differentiated capillary | Negativity for all markers and low expression of pan-endothelial EC markers | | | | | • | ● |
| | 6 | Intralobular venule | *PTGDS, RAMP3, SULT1E1, TAGLN, C7* | | | | | ● | • |
| | 7 | Bronchial capillary | *ANGPT2, HISPA1B, CD34* | | | | | ● | • |
| | 8 | Aerocyte (aCAP) | *AFF3, IL1R1, PRKG1, NCALD, HPGD* | | | | | • | ● |
| | 9 | Inflammatory | *IL6, SELE, ICAM1* | | | | | ● | · |
| | 10 | De-differentiated venule | *NAPSA, SFTPB, SFTPA1, SLPI, SFTPA2, PGC* | | | | | • | · |
| | 11 | De-differentiated arteriole | *HLA-DPB1, C1QB, HLA-DRA, C1QA, C1QC, ALOX5AP, LYZ, TYROBP* | | | | | · | · |

**b**

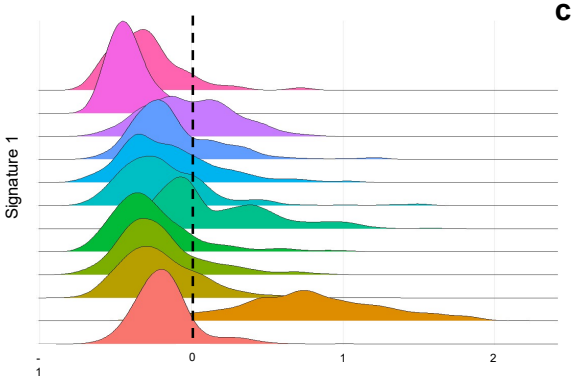


**c**

| BEC sub-cluster | Sig1 | Sig2 | Sig3 | Sig4 | Sig6 | Sig7 | Sig8 | Sig9 | Sig10 | Sig11 |
|---|---|---|---|---|---|---|---|---|---|---|
| 0 | -0.167 | -0.078 | 0.116 | 0.008 | -0.011 | -0.005 | 0.104 | -0.060 | 0.596 | 0.069 |
| 1 | 0.727 | 0.027 | -0.444 | -0.096 | -0.130 | -0.195 | -0.303 | -0.135 | -0.421 | -0.196 |
| 2 | -0.133 | 0.654 | -0.418 | -0.143 | 0.204 | -0.005 | -0.277 | -0.127 | -0.117 | -0.041 |
| 3 | -0.213 | -0.271 | 1.102 | -0.002 | -0.145 | -0.152 | 0.143 | 0.001 | 0.111 | -0.113 |
| 4 | -0.256 | -0.269 | -0.302 | 0.707 | -0.081 | -0.064 | -0.288 | -0.026 | 0.181 | -0.194 |
| 5 | 0.145 | -0.007 | 0.008 | -0.051 | -0.061 | -0.089 | -0.008 | -0.135 | -0.120 | 0.141 |
| 6 | -0.156 | -0.233 | -0.010 | -0.146 | 1.010 | -0.184 | -0.240 | -0.007 | 0.293 | -0.129 |
| 7 | -0.141 | -0.099 | -0.167 | -0.100 | -0.049 | 0.844 | -0.199 | 0.135 | 0.099 | -0.170 |
| 8 | -0.126 | -0.231 | -0.114 | -0.149 | -0.239 | -0.203 | 1.170 | -0.102 | -0.083 | 0.115 |
| 9 | -0.011 | -0.013 | -0.254 | -0.085 | 0.398 | 0.227 | -0.177 | 0.983 | 0.650 | -0.119 |
| 10 | -0.380 | -0.302 | -0.226 | -0.119 | -0.164 | -0.120 | -0.190 | -0.290 | 3.147 | -0.033 |
| 11 | -0.286 | -0.280 | -0.155 | -0.130 | -0.177 | -0.056 | -0.205 | -0.343 | -0.003 | 1.348 |

**d**

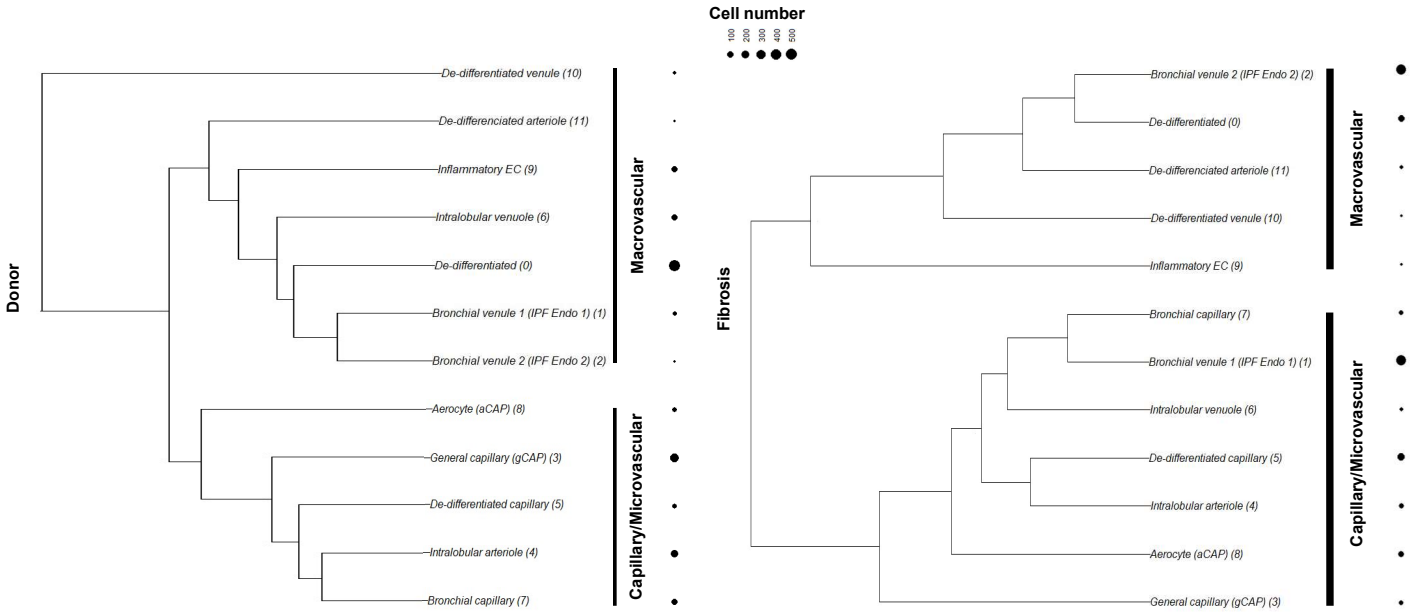

medRxiv preprint doi: https://doi.org/10.1101/2022.03.08.22272025; this version posted March 10, 2022. The copyright holder for this preprint **(which was not certified by peer review)** is the author/funder, who has granted medRxiv a license to display the preprint in perpetuity.
It is made available under a CC-BY-NC-ND 4.0 International license .

# FIGURE 5

**a**

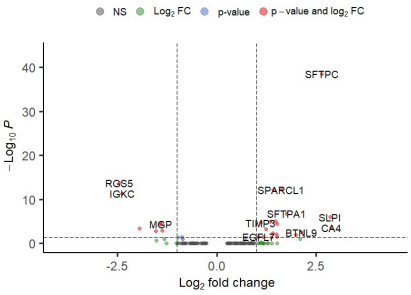


**b**

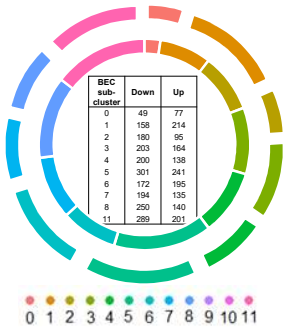


| BEC sub-cluster | Down | Up |
|---|---|---|
| 0 | 49 | 77 |
| 1 | 158 | 214 |
| 2 | 180 | 95 |
| 3 | 203 | 164 |
| 4 | 200 | 138 |
| 5 | 301 | 241 |
| 6 | 172 | 195 |
| 7 | 194 | 135 |
| 8 | 250 | 140 |
| 11 | 289 | 201 |

**c**

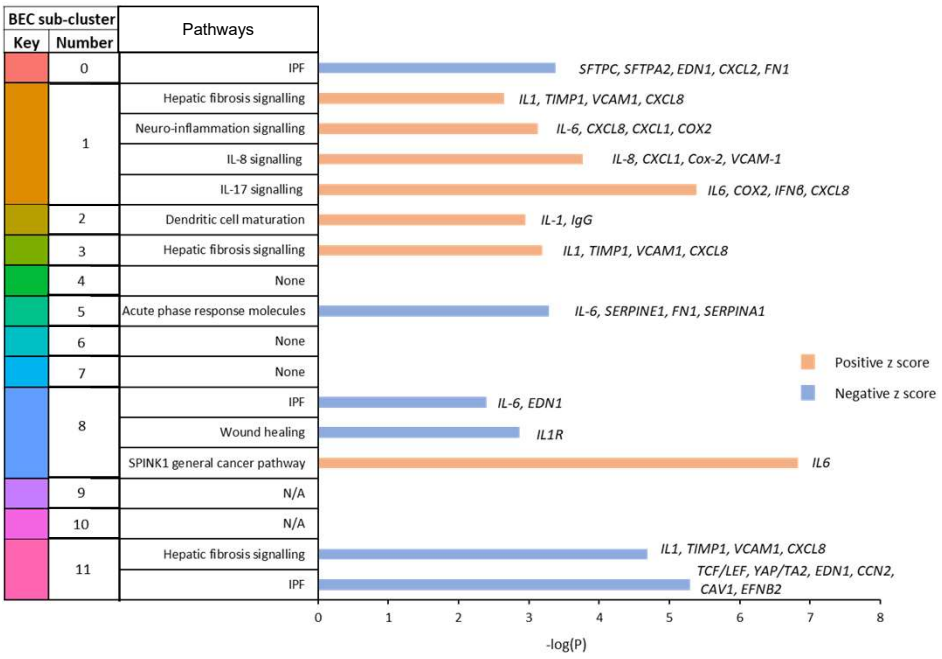


**d**

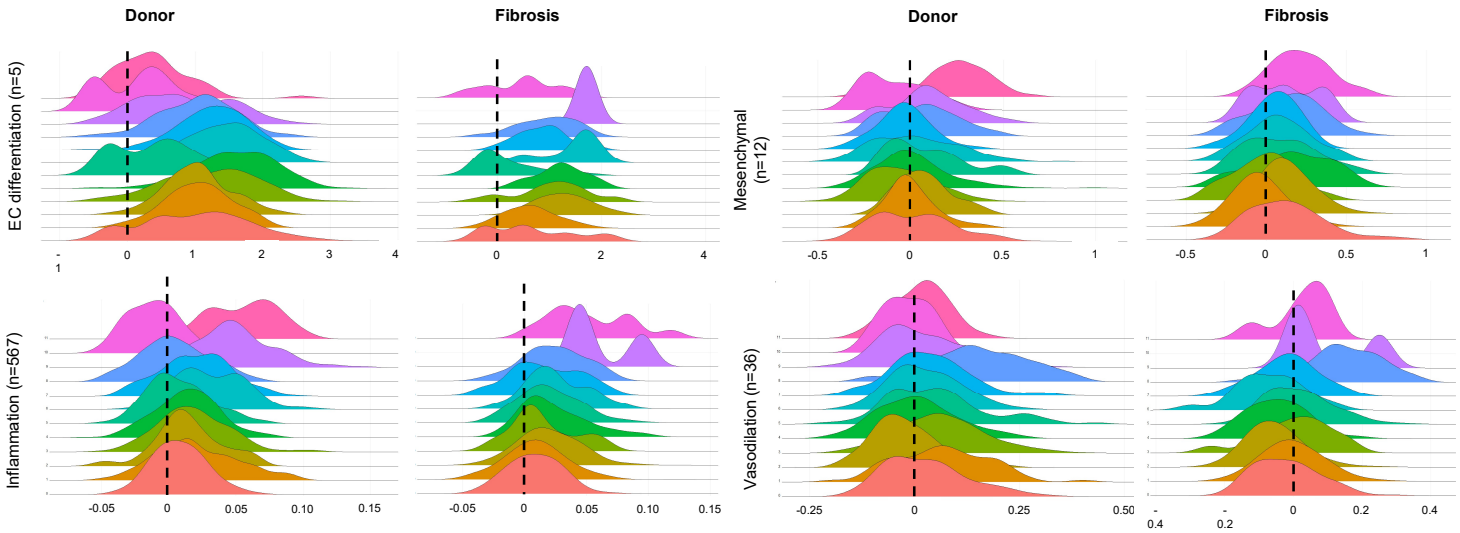


**e**

| BEC sub-cluster | | | Cell Process | | | | | | | | | |
|---|---|---|---|---|---|---|---|---|---|---|---|---|
| Key | Number | Annotation | EC Differentiation | Mesenchymal | Senescence | Apoptosis | Proliferation | Migration | Angiogenesis | Inflammation | Vasodilation | Permeability |
| | 0 | De-differenting vascular EC | <0.001 | <0.001 | NS | 0.032 | NS | 0.008 | NS | NS | <0.001 | 0.014 |
| | 1 | IPF Endo 1 (VE Peribronchial) | <0.001 | 0.038 | NS | <0.001 | 0.011 | <0.001 | 0.025 | 0.007 | <0.001 | <0.001 |
| | 2 | IPF Endo 2 (Bronchial EC) | 0.002 | 0.041 | NS | <0.001 | NS | 0.029 | <0.001 | NS | 0.006 | <0.001 |
| | 3 | General capillary (gCAP) | NS | NS | NS | 0.007 | 0.007 | NS | 0.019 | NS | 0.011 | NS |
| | 4 | Intralobular arteriole | <0.001 | <0.001 | NS | 0.043 | NS | 0.0041 | NS | NS | <0.001 | NS |
| | 5 | De-differenciated capillary | 0.004 | NS | 0.017 | 0.005 | NS | NS | NS | 0.001 | 0.016 | 0.032 |
| | 6 | Intralobular venule | NS | NS | NS | NS | <0.001 | NS | NS | NS | <0.001 | NS |
| | 7 | Bronchial capillary | <0.001 | 0.001 | NS | NS | 0.019 | NS | NS | NS | 0.005 | 0.016 |
| | 8 | Aerocyte (aCAP) | ns | 0.026 | 0.01 | NS | <0.001 | <0.001 | NS | <0.001 | NS | NS |
| | 9 | Inflammatory EC | N/A | N/A | N/A | N/A | N/A | N/A | N/A | N/A | N/A | N/A |
| | 10 | Subsegmental vein | N/A | N/A | N/A | N/A | N/A | N/A | N/A | N/A | N/A | N/A |
| | 11 | Subsegmental artery | N/A | N/A | N/A | N/A | N/A | N/A | N/A | N/A | N/A | N/A |